

LOCALLY BIASED GALAXY FORMATION AND LARGE SCALE STRUCTURE

Vijay K. Narayanan, Andreas A. Berlind, and David H. Weinberg
Department of Astronomy, The Ohio State University, Columbus, OH 43210;
Email: vijay,aberlind,dhw@astronomy.ohio-state.edu

ABSTRACT

We examine the influence of the morphology-density relation and a wide range of simple models for biased galaxy formation on statistical measures of large scale structure. We contrast the behavior of local biasing models, in which the efficiency of galaxy formation is determined by the density, geometry, or velocity dispersion of the local mass distribution, with that of non-local biasing models, in which galaxy formation is modulated coherently over scales larger than the galaxy correlation length. If morphological segregation of galaxies is governed by a local morphology-density relation, then the correlation function of E/S0 galaxies should be steeper and stronger than that of spiral galaxies on small scales, as observed, while on large scales the E/S0 and spiral galaxies should have correlation functions with the same shape but different amplitudes. Similarly, all of our local bias models produce scale-independent amplification of the correlation function and power spectrum in the linear and mildly non-linear regimes; only a non-local biasing mechanism can alter the shape of the power spectrum on large scales. Moments of the biased galaxy distribution retain the hierarchical pattern of the mass moments, but biasing alters the values and scale-dependence of the hierarchical amplitudes S_3 and S_4 . Pair-weighted moments of the galaxy velocity distribution are sensitive to the details of the bias prescription even if galaxies have the same local velocity distribution as the underlying dark matter. The non-linearity of the relation between galaxy density and mass density depends on the biasing prescription and the smoothing scale, and the scatter in this relation is a useful diagnostic of the physical parameters that determine the bias. While the assumption that galaxy formation is governed by local physics leads to some important simplifications on large scales, even local biasing is a multi-faceted phenomenon whose impact cannot be described by a single parameter or function. The sensitivity of galaxy clustering statistics to the details of galaxy biasing is an obstacle to testing cosmological models, but it is an equally significant asset for testing physical theories of galaxy formation against data from redshift and peculiar velocity surveys.

Subject headings: galaxies: clustering, large scale structure of the Universe

1. Introduction

Within a decade of defining his classification system for galaxies, Hubble (1936) observed that elliptical and spiral galaxies tend to reside in different environments, with elliptical galaxies preferentially represented in rich clusters and spiral galaxies more numerous in the field. More recent studies have confirmed and detailed this dependence of clustering on morphological type, and they have shown that luminous galaxies cluster more strongly than faint galaxies (e.g., Hamilton 1988; Park et al. 1994; Loveday et al. 1995; Benoist et al. 1996; Willmer, da Costa & Pellegrini 1998) and that optically selected galaxies cluster more strongly than infrared selected galaxies (e.g., Lahav, Nemiroff, & Piran 1990; Saunders, Rowan-Robinson & Lawrence 1992; Peacock & Dodds 1994). At most one of these galaxy populations can trace the underlying distribution of mass, and it is more likely that none of them does. The idea of biased galaxy formation — preferential formation of galaxies in high density environments — was originally introduced with the hope of reconciling the low apparent mass-to-light ratios of bound galaxy structures with the theoretically motivated assumption of an $\Omega = 1$ universe (Davis et al. 1985; Bardeen et al. 1986). However, it is now broadly recognized that bias, or anti-bias, is a possibility that we are stuck with, whatever the value of Ω . Cosmological N-body simulations can predict statistical properties of the mass distribution in a specified cosmological model, but they cannot predict the clustering of galaxies without an additional prescription for the relation between galaxies and mass. In this paper, we apply a variety of simple bias prescriptions to N-body simulations in order to see how assumptions about bias influence measurable properties of large scale structure, such as the correlation function, the power spectrum, moments of galaxy counts, pairwise velocities, and the relation between galaxy density and peculiar velocity fields.

While the full theory of galaxy formation is likely to be complicated, a plausible and still very general assumption is that the efficiency of galaxy formation is determined by properties of the local environment. For practical purposes, “local” means a scale comparable to the galaxy correlation length, the distance over which material in non-linear structures has mixed during the history of the universe. In a local theory of galaxy formation, when a collapsing region of the mass distribution decides whether to become a galaxy (or what type of galaxy to become, or how many galaxies to become), it has no direct knowledge of material that it has never encountered. On the other hand, “non-local” biasing, in which the efficiency of galaxy formation varies coherently over larger scales, requires a more exotic physical mechanism, such as suppression or stimulation of galaxy formation by ionizing radiation or by some other influence that can propagate at the speed of light. In this paper, we examine several examples of local biasing, with the efficiency of galaxy formation determined by the density, pressure, or geometry of the mass distribution in a surrounding $4h^{-1}$ Mpc sphere (where $h \equiv H_0/100 \text{ km s}^{-1} \text{ Mpc}^{-1}$). We compare the effects of these local bias models to those of non-local models inspired by the proposals of Babul & White (1991) and Bower et al. (1993).

For purposes of our study, it is important to maintain the distinction between a model of biased galaxy formation, which is a fully specified prescription for populating a mass distribution

with galaxies, and a description of the *effects* of bias. The widely used “linear bias model” — $\delta_g = b\delta_m$, where $\delta_m \equiv \rho/\bar{\rho} - 1$ is the mass density contrast, δ_g is the galaxy density contrast, and b is the bias factor — is more properly regarded as a description rather than a model. One cannot use the $\delta_g = b\delta_m$ formula to assign galaxies to the mass distribution on any scale where the minimum density contrast is $\delta_{m,\min} < -1/b$, since it would demand an unphysically negative galaxy density. However, linear bias could emerge as a reasonable approximation to the effects of a physical bias model on large scales, at least for some purposes. The relation between the galaxy and mass correlation functions is often written $\xi_g(r) = b^2(r)\xi_m(r)$, which is again a description rather than a model. While it might seem reasonable to let $b(r)$ be an arbitrary function of scale, a series of analytic arguments of increasing generality suggest that for any local bias the quantity $b(r)$ must asymptote to a constant value in the limit $\xi(r) \ll 1$, making it impossible for local bias to resolve a discrepancy between the predicted and observed shapes of $\xi(r)$ on large scales (Coles 1993; Fry & Gaztañaga 1993; Gaztanaga & Baugh 1998; Scherrer & Weinberg 1998). Even the most general of these arguments relies on assumptions about the mass clustering and the bias model, and it yields only an asymptotic result. The numerical approach here complements the analytic studies by exhibiting fully non-linear solutions for a diverse set of biasing models, including some that do not satisfy the formal assumptions of the analytic calculations.

In principle, the relation between galaxies and mass should be a prediction of a cosmological theory, not an input to it. There has been substantial progress towards making such *a priori* predictions in recent years using hydrodynamic simulations (Cen & Ostriker 1992, 1993, 1998; Katz, Hernquist, & Weinberg 1992, 1996, 1998; Blanton et al. 1998), N-body simulations that attempt to resolve galaxy mass halos within larger virialized systems (Colín et al. 1998), or a combination of lower resolution N-body simulations with semi-analytic models of galaxy formation (Kauffmann et al. 1997, 1998; Governato et al. 1998). However, the semi-analytic models require a series of approximations and assumptions, and the numerical studies suffer from limited resolution and simulation volumes and also rely on simplified descriptions of star formation and supernova feedback. At present these approaches yield physically motivated models of biased galaxy formation that can be tested against observations, but they do not provide definitive predictions.

In this paper we take a different and in some ways less ambitious tack. We combine large volume, relatively low resolution N-body simulations with simple bias prescriptions that are deliberately designed to “parametrize ignorance” about galaxy formation, by illustrating a wide range of possibilities. We extend Weinberg’s (1995) study along similar lines by using better simulations and examining a much wider range of galaxy clustering measures. Our study also overlaps that of Mann, Peacock, & Heavens (1998, hereafter MPH98), who applied several different biasing prescriptions to large N-body simulations and investigated their influence on the galaxy power spectrum and on cluster mass-to-light ratios. Our goal here is to see which measurable properties of galaxy clustering are sensitive to assumptions about bias and which properties are robust, or at least are affected in a simple way by local bias. Our numerical study complements

the general analytic treatment of non-linear, stochastic biasing models by Dekel & Lahav (1998, hereafter DL98).

The biasing prescriptions that we adopt in this paper are all Eulerian models, meaning that the efficiency of galaxy formation is determined by properties of the evolved mass density field. These can be contrasted with Lagrangian bias models, such as the high peaks model (Davis et al. 1985; Bardeen et al. 1986), in which the efficiency of galaxy formation depends on the initial (linear) density field. Because galaxies can merge as structure evolves, neither a pure Lagrangian nor a pure Eulerian description of bias is entirely realistic. However, for studies of galaxy clustering at a specified redshift, either approach may provide a reasonable approximate description, and the distinction between them is more technical than physical. The distinction between local and non-local models, on the other hand, is fundamentally tied to the physical mechanisms that cause bias. Eulerian, Lagrangian, and intermediate approaches would yield different predictions for the evolution of bias with redshift, but we do not examine this issue in this paper. The evolution of bias has been studied using the numerical and semi-analytic approaches mentioned above and in a more general analytic framework by Fry (1996) and Tegmark & Peebles (1998).

We begin our investigation in §2 with a simple but informative example, in which the galaxy population as a whole traces the mass but the mix of morphological types is determined by a local morphology-density relation. This example illustrates some general properties of local bias models, and our calculations provide generic predictions, testable with the next generation of redshift surveys, for the dependence of the large scale correlation function and power spectrum on morphological type. We then move to models in which the galaxy population has an overall bias, which is applied using a variety of local and non-local prescriptions. We describe the models and examine their influence on a number of different measures of large scale structure in §3. Section 4 provides a fairly complete summary of our results and discusses their implications in light of other recent studies and anticipated observational developments.

2. The Morphology-Density Relation and the Large Scale Clustering of Galaxy Types

The longest recognized and most clearly established form of “bias” in the galaxy distribution is the marked preference of early-type galaxies for dense environments (Hubble 1936; Zwicky 1937; Abell 1958). There have been numerous efforts to quantify this connection between morphology and environment (e.g., Dressler 1980; Postman & Geller 1984; Lahav & Saslaw 1992; Whitmore, Gilmore, & Jones 1993), and several groups have used angular correlation functions, redshift-space correlation functions, or de-projected real-space correlation functions to characterize the dependence of clustering on morphology (Davis & Geller 1976; Giovanelli, Haynes & Chincarini 1986; Loveday et al. 1995; Guzzo et al. 1997; Willmer, da Costa & Pellegrini 1998). The stronger clustering of early-type galaxies explains the stronger clustering found in optically selected galaxy catalogs relative to IRAS-selected catalogs, which preferentially include

dusty, late-type galaxies (Babul & Postman 1990). Postman & Geller (1984, hereafter PG84) parametrize the morphology-environment connection as a relation between morphological fractions and local galaxy density: for overdensities $\rho_g/\bar{\rho}_g \lesssim 100$ the fractions of ellipticals, S0s, and spirals are independent of environment, but at higher densities the elliptical and S0 fractions climb steadily, eventually saturating for $\rho_g/\bar{\rho}_g \gtrsim 10^5$. In this Section, we consider a model in which the galaxy population as a whole traces the underlying mass distribution but morphological types are assigned according to PG84’s prescription. Our results will show what should be expected from large redshift surveys like the 2 Degree Field (2dF) survey (Colless 1998) and the Sloan Digital Sky Survey (SDSS; Gunn & Weinberg 1995) if a local morphology-density relation is a correct description of the influence of environment on morphological type. This investigation also provides a “warmup” for the investigations in §3, since the morphology-density relation is a simple example of a local bias mechanism.

For our underlying mass distribution, we use the output of an N-body simulation of an open cold dark matter (CDM) model performed by Cole et al. (1998, hereafter CHWF98). The cosmological parameters are $\Omega_m = 0.4$, $\Omega_\Lambda = 0$, $\Gamma = 0.25$, $n = 1$, where $\Gamma \equiv \Omega_m h \exp(-\Omega_b - \Omega_b/\Omega_m)$ (Sugiyama 1995), $\Omega_m, \Omega_b, \Omega_\Lambda$ are the matter, baryon, and vacuum energy density parameters, and $n = 1$ implies a scale-invariant inflationary power spectrum. The model is cluster-normalized (White, Efstathiou, & Frenk 1993; Eke, Cole & Frenk 1996) and has an rms mass fluctuation $\sigma_8 = 0.95$ in spheres of radius $8h^{-1}$ Mpc. The amplitude σ_8 is related to the linear theory power spectrum $P(k)$ by

$$\sigma_8^2 = \int_0^\infty 4\pi k^2 P(k) \widetilde{W}^2(kR) dk, \quad (1)$$

where $\widetilde{W}(kR)$ is the Fourier transform of a spherical top hat filter with radius $R = 8h^{-1}$ Mpc. The CHWF98 simulation uses a modified version of the AP3M code of Couchman (1991) to follow the gravitational evolution of 192^3 particles in a periodic cubical box of side $345.6h^{-1}$ Mpc. The gravitational force softening is $\epsilon = 90h^{-1}$ kpc comoving (for a Plummer force law) and the particle mass is $m_p = 6.47 \times 10^{11} h^{-1} M_\odot$. Further details of the simulation are given in CHWF98; this is their model O4S.

Our implementation of the morphology-density relation is based loosely on figures 1 and 2 of PG84. We assign each particle in the simulation a density equal to the mean density in a sphere enclosing its five nearest neighbors. We assign the particle a spiral (Sp), S0, or elliptical (E) morphological type at random, with relative probabilities $F_{\text{Sp}}, F_{\text{S0}}, F_{\text{E}}$ that depend on the density. For $\rho < \rho_F = 100\bar{\rho}$, the morphological fractions are $F_{\text{Sp}} = 0.7$, $F_{\text{S0}} = 0.2$, $F_{\text{E}} = 0.1$. For $\rho_F < \rho < \rho_C = 6 \times 10^4 \bar{\rho}$, the fractions are

$$\begin{aligned} F_{\text{Sp}} &= 0.7 - 0.6\alpha \\ F_{\text{S0}} &= 0.2 + 0.3\alpha \\ F_{\text{E}} &= 1 - F_{\text{Sp}} - F_{\text{S0}} \\ \alpha &= \log_{10}(\rho/\rho_F) / \log_{10}(\rho/\rho_C). \end{aligned} \quad (2)$$

For $\rho > \rho_C$, the morphological fractions saturate at $F_{\text{Sp}} = 0.1$, $F_{\text{S0}} = 0.5$, $F_{\text{E}} = 0.4$. With this formulation, 13.7% of the particles are classified as ellipticals, 23.7% as S0s, and the remaining 62.6% as spirals. Changes to ρ_F or ρ_C or the density assignment method would alter the numerical values of the bias parameters discussed below, but they would not change our results in a qualitative way.

Figure 1 compares the spatial distributions of the different types of galaxies. The full galaxy population, a random subset of the N-body particles with space density $n_g = 0.01h^3 \text{ Mpc}^{-3}$, is shown in panel (a). For panels (b)-(d), we have artificially boosted the selection probabilities so that each morphological sub-population has density $0.01h^3 \text{ Mpc}^{-3}$; the visual differences among the panels therefore reflect the differences in the clustering strengths of the galaxy types rather than their different number densities. For our adopted parameters, these visual differences are rather subtle, though the contrast between clusters and voids is more noticeable for the ellipticals (panel b) than for the spirals (panel d), as expected.

Figure 2 (top panel) compares the two-point correlation functions $\xi(r)$ of the three galaxy populations to the two-point correlation function of the mass distribution, which is equal to that of the full galaxy population by construction. For $r \lesssim 4h^{-1} \text{ Mpc}$, the correlation functions of the E and S0 galaxies are both stronger and steeper than that of the spiral galaxies, which is just the behavior found in observational studies of the angular and spatial correlation functions of different galaxy types (Davis & Geller 1976; Giovanelli et al. 1986; Loveday et al. 1995; Guzzo et al. 1997; Willmer et al. 1998). If one were to fit power laws to these correlation functions and extrapolate to large r , they would cross at $r \sim 10h^{-1} \text{ Mpc}$, with the early-type galaxies more weakly clustered at large scales. The true behavior in the simulation is quite different, however. At $r \gtrsim 4h^{-1} \text{ Mpc}$, the shape of the $\xi(r)$ of the early-type galaxies changes to match that of the spirals, and the amplitude of $\xi(r)$ for the early-type galaxies is higher at all scales. The large scale behavior is consistent with the observational measurements cited above, but these do not have sufficient precision at large r to clearly show the E, S0, and spiral correlation functions tracing each other with a constant logarithmic offset. The prediction that the large scale shape of $\xi(r)$ is independent of morphological type should be easily testable with the 2dF and SDSS redshift surveys.

The bottom panel in Figure 2 shows the bias function $b_\xi(r)$, defined as

$$b_\xi(r) = \sqrt{\frac{\xi_g(r)}{\xi_m(r)}}, \quad (3)$$

where $\xi_g(r)$ and $\xi_m(r)$ are the correlation functions of the galaxy and the mass distributions, respectively. This function becomes independent of scale beyond about $4h^{-1} \text{ Mpc}$, and it settles at a different level for each of the galaxy types. We will show in §3 below that this constancy of $b_\xi(r)$ at large r is a generic feature of local biasing models. The early-type galaxies are always positively biased with respect to the mass distribution, $b_\xi(r) > 1$, while the spirals are anti-biased on all scales, $b_\xi(r) < 1$. The clustering amplitude of the elliptical galaxies on large scales is a factor of 1.3 larger than that of the spiral galaxies, consistent with the ratio derived using the galaxies

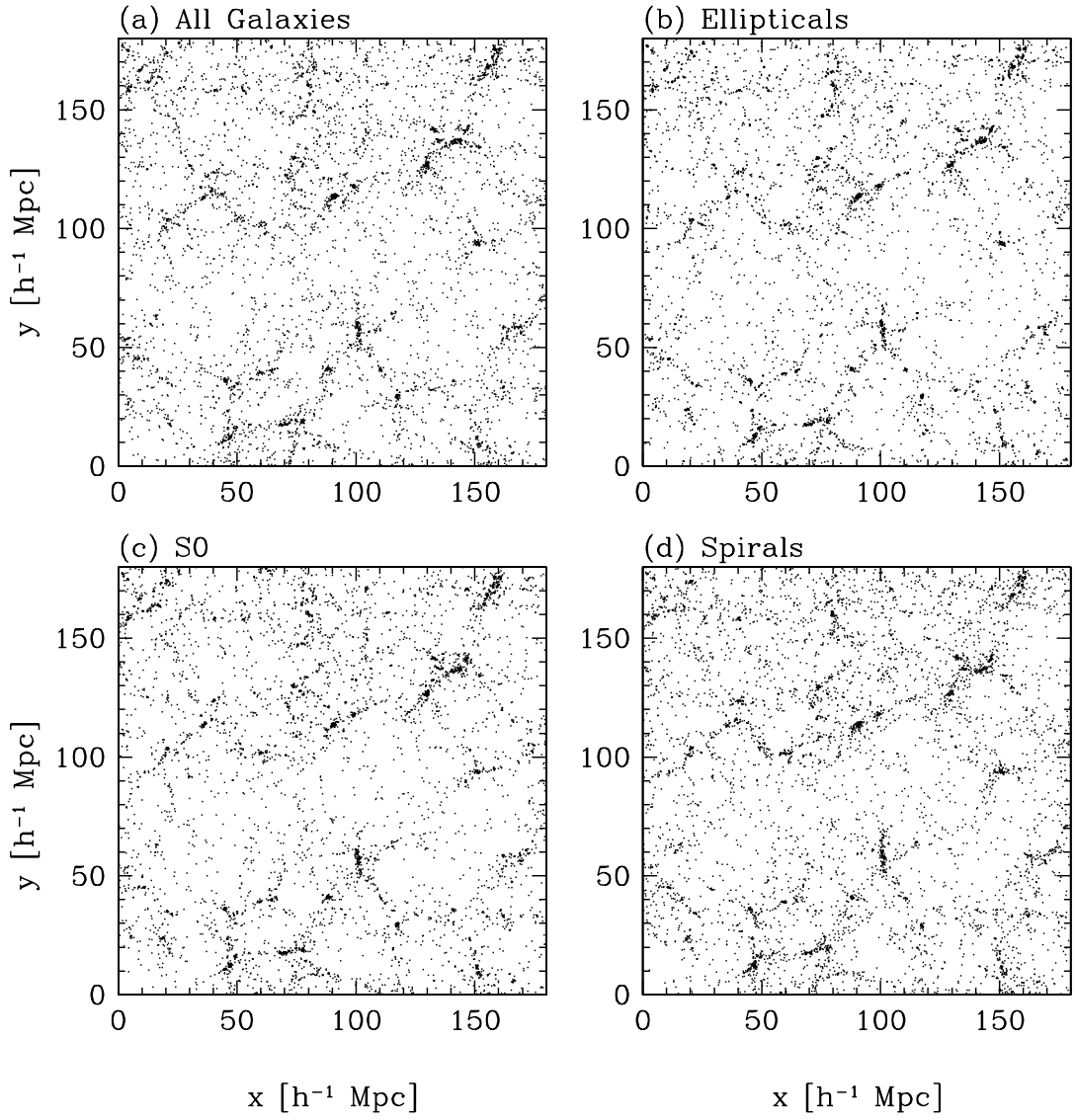


Fig. 1.— Galaxy distributions from a local morphology-density relation. The panels show the galaxy distributions in a slice $18h^{-1}\text{Mpc}$ thick and spanning $180h^{-1}\text{Mpc}$ in the other two dimensions. (a) Underlying mass distribution. The remaining panels show the galaxy distributions traced by (b) ellipticals, (c) S0s, and (d) spirals. All of the galaxy distributions have been sampled to the same number density of $0.01h^3\text{Mpc}^{-3}$, so that visual differences reflect differences in clustering rather than differences in galaxy density.

in the Stromlo-APM redshift survey (Loveday et al. 1995). The bias of the early-type galaxies increases towards smaller scales, while that of the spirals decreases. The increase in the relative clustering strength of ellipticals and spirals towards smaller scales is observed in the clustering analysis of the Southern Sky Redshift Survey (Willmer et al. 1998). The bias of the full galaxy population is $b_{\xi}(r) = 1$ by construction.

The top panel of Figure 3 shows the power spectra, $P(k)$, of the mass and the galaxy distributions. We form continuous density fields by cloud-in-cell (CIC) binning the discrete particle distributions onto a 192^3 grid, and compute $P(k)$ using a Fast Fourier Transform (FFT). We sample all the galaxy distributions to the same number density of $0.01h^3\text{Mpc}^{-3}$, so all the power spectra have the same shot noise contribution. The amplification of the clustering of early-type galaxies and suppression of the clustering of spiral galaxies is similar to that seen in Figure 2, but the $P(k)$ plot better reveals the behavior on the largest scales. The bottom panel shows the bias functions in Fourier space, $b_P(k)$, defined as

$$b_P(k) = \sqrt{\frac{P_g(k)}{P_m(k)}}, \quad (4)$$

where $P_g(k)$ and $P_m(k)$ are the power spectra of the galaxy and the mass distributions, respectively. This bias function also becomes independent of scale on large scales and has the same relative behavior as $b_{\xi}(r)$ for the different galaxy types.

The assignment of morphological types based on local density produces a difference in the clustering strength of different galaxy types at *all* scales. The reason for the large scale bias is the same one identified by Kaiser (1984) in his discussion of cluster correlations: regions that are highly overdense on small scales tend to reside in regions where the large scale, background density is also high. The bias functions in Figures 2 and 3 are scale-dependent in the regime where clustering is non-linear, but they asymptote to constant values on large scales. We will soon see that this behavior is a generic property of local biasing models.

We have assumed in this Section that the galaxy population as a whole traces the mass, but we would expect the relative clustering of different galaxy types to be similar even if the galaxy population has a net bias or anti-bias, at least if the mechanism that produces that bias is local. While the numerical values of the relative bias parameters depend on our choices of ρ_F and ρ_C (eq. [2]) and our method of defining the local density, the qualitative prediction that the correlation functions and power spectra of E, S0, and spiral galaxies have the same shape at large scales should hold in any model where the morphological type is determined by the local density.

3. The Influence of Bias on Galaxy Clustering

If the environment influences the formation efficiency of individual galaxy types, then it is likely to influence the overall efficiency of galaxy formation as well. While we are far from having a

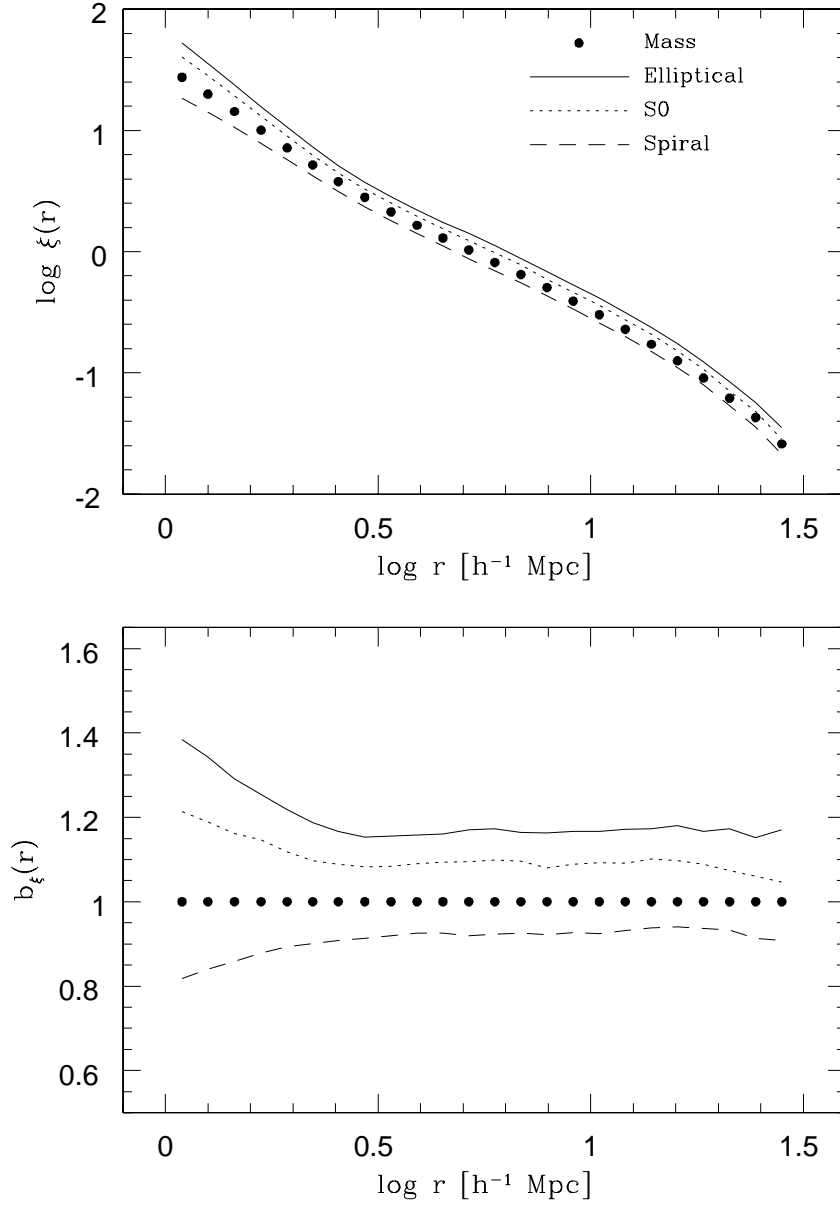


Fig. 2.— Top: Correlation functions of the galaxy distributions of different types of galaxies, with morphological types assigned according to a local morphology-density relation. Bottom: The bias functions $b_\xi(r)$ defined in equation (3).

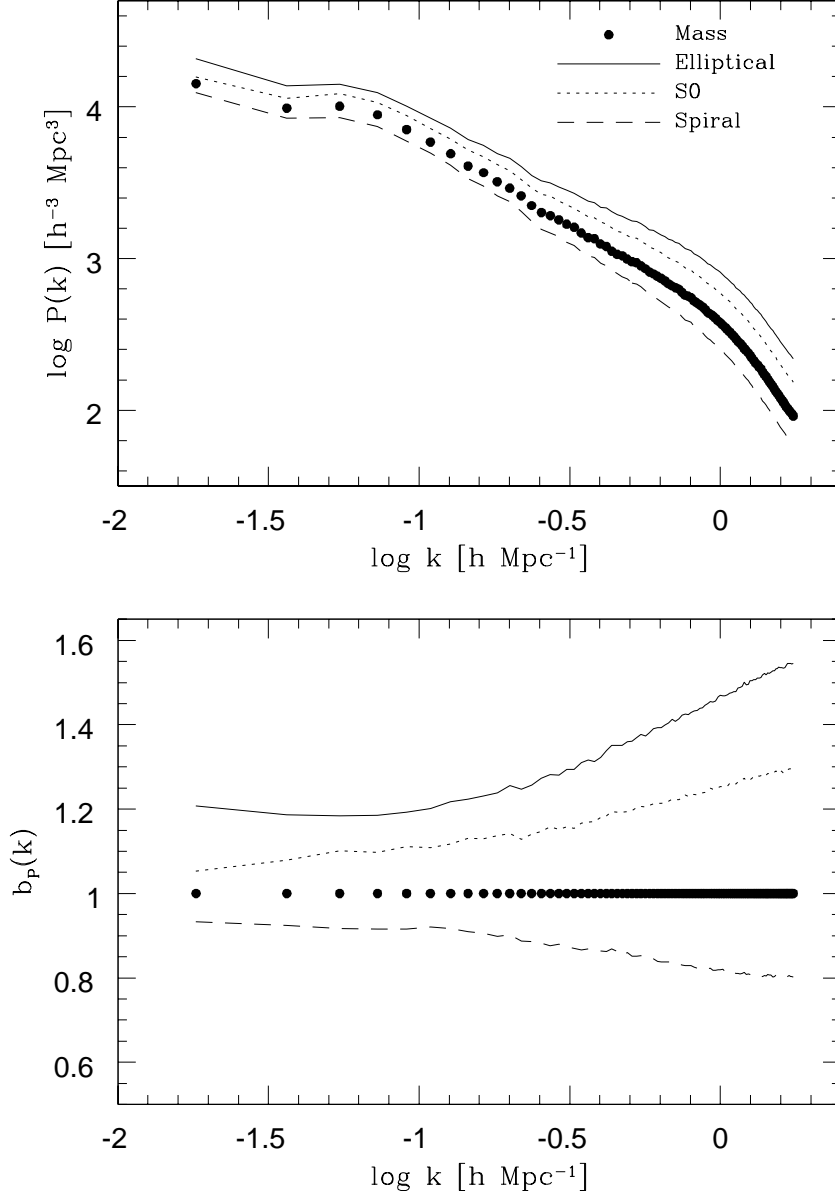


Fig. 3.— Top: Power spectra of the galaxy distributions of different types of galaxies, with morphological types assigned according to a local morphology-density relation. Bottom: The bias functions $b_P(k)$ defined in equation (4). The largest scale plotted, $k = 0.018h \text{ Mpc}^{-1}$, is the fundamental mode of the $345.6h^{-1} \text{ Mpc}$ simulation cube.

definitive theoretical account of galaxy formation, the numerical and semi-analytic studies cited in §1 suggest that galaxies should be significantly biased tracers of structure, at least in some regimes of luminosity and redshift. With the morphology-density results as background, we now turn to a much broader set of biasing models, some local and some non-local. We no longer attempt to discriminate among galaxy types but instead consider models in which the galaxy population as a whole is biased with respect to the underlying mass distribution.

For our underlying model (described in §3.1), we adopt an $\Omega = 1$, tilted CDM model. This model has an rms mass fluctuation amplitude $\sigma_8 = 0.55$, about a factor of two below the observed fluctuation amplitude of bright optical galaxies (e.g., Davis & Peebles 1983; Loveday et al. 1995). We apply a number of different local and non-local Eulerian biasing prescriptions (described in §3.2 and §3.3) to this model, each of which has a single adjustable parameter that controls the strength of the bias. We choose the value of this parameter by requiring that the ratio of rms galaxy fluctuations to rms mass fluctuations,

$$b_\sigma = \frac{\sigma_g(R)}{\sigma_m(R)}, \quad (5)$$

is $b_\sigma = 2$ in spheres of radius $R = 12h^{-1}$ Mpc. The definition of the bias factor in equation (5) is identical to the quantity b_{var} defined by DL98. We fix the bias factor at $R = 12h^{-1}$ Mpc rather than $R = 8h^{-1}$ Mpc so that our local bias models have similar bias at very large scales. We sample the biased galaxy distributions to an average density of $0.01h^3\text{Mpc}^{-3}$, so that all of the galaxy distributions have comparable shot-noise properties.

3.1. Mass Distribution

In all of the Eulerian biasing schemes that we study in this paper, we choose the galaxies from the underlying mass distribution of a tilted CDM model with $\Omega_m = 1, \Omega_\Lambda = 0$, and $\Omega_b = 0.05$. The primordial slope of the power spectrum, n , is adjusted to simultaneously match the CMB anisotropies on large scales and the observed masses of galaxy clusters on small scales. The cluster constraint requires $\sigma_8 = 0.55$ (White et al. 1993), which implies $n = 0.803$ if one incorporates the standard inflationary prediction for gravitational wave contributions to the COBE anisotropies. We compute the CDM transfer function using the analytical fitting functions provided by Eisenstein & Hu (1998).

Our model parameters are the same as those of the E2 model of Cole et al. (1997, see also CHWF98). However, for the purposes of our investigation it is more important to have good statistics on very large scales than to have high gravitational force resolution. We therefore perform our own N-body simulations of this model using a particle-mesh (PM) N-body code written by C. Park, which is described and tested by Park (1990; see also Park 1991). Each simulation uses 200^3 particles and a 400^3 force mesh to follow the gravitational evolution in a periodic cube $400h^{-1}$ Mpc on a side. We start the gravitational evolution from a redshift $z = 20$ and follow it to

$z = 0$ in 80 equal incremental steps of the expansion scale factor $a(t)$. We also evolved this mass distribution using twice this number of time steps and found that the correlation function and the velocity dispersion of the resulting mass distributions changed very little, showing that our results are robust to increasing the temporal resolution of the N-body simulation. We ran four such simulations with different random phases for the Fourier components of the initial density field, and the results we show are averaged over these four independent mass/galaxy distributions.

3.2. Local Biasing Schemes

We now describe our local Eulerian biasing models in detail. The first two schemes, density-threshold bias and power-law bias, select galaxies based on the local mass density alone. The sheet bias scheme selects galaxies based on the geometry of the local mass distribution. We also investigated two other local bias schemes, one based on pressure and one on geometry, that we will omit from our detailed presentation of results because they prove very similar to the density-threshold and sheet bias schemes, respectively. We compute all the local properties associated with a mass particle, including the local mass density and the moment of inertia tensor, in a sphere of radius $4h^{-1}\text{Mpc}$ around that particle.

3.2.1. Density-threshold bias

In order for galaxies to have a net bias $b_\sigma > 1$, they should preferentially populate regions of higher mass density. The simplest prescription that achieves this is a density-threshold bias: galaxy formation is entirely suppressed below some threshold, and galaxies form with equal efficiency per unit mass in all regions above the threshold. This biasing scheme was adopted in some of the early numerical investigations of CDM models (e.g., Melott & Fry 1986), and it has been used extensively by J. Einasto and collaborators in theoretical modeling of voids and superclusters (e.g., Einasto et al. 1994). In the density-threshold bias model, the probability that a particle with local mass density ρ_m is selected as a galaxy is

$$P = \begin{cases} A & \text{if } \rho_m \geq B, \\ 0 & \text{if } \rho_m < B. \end{cases} \quad (6)$$

We choose the threshold density B so that the bias factor $b_\sigma(12h^{-1} \text{Mpc}) = 2$ (eq. [5]) and the probability A so that the mean galaxy density is $n_g = 0.01h^3 \text{Mpc}^{-3}$.

3.2.2. Power-law bias

The threshold model is extreme in the sense that galaxy formation is completely suppressed at low densities and independent of density above the threshold. In our second model, we make the

galaxy density a steadily increasing, power-law function of the mass density, $(\rho_g/\bar{\rho}_g) \propto (\rho_m/\bar{\rho}_m)^B$. The selection probability for a particle with local mass density ρ_m to become a galaxy is therefore

$$P = A(\rho_m/\bar{\rho}_m)^{B-1}. \quad (7)$$

We choose the value of B so that $b_\sigma = 2$ and the value of A so that $n_g = 0.01h^3\text{Mpc}^{-3}$. This biasing relation is similar to the one suggested by Cen & Ostriker (1993) based on hydrodynamic simulations incorporating physical models for galaxy formation (Cen & Ostriker 1992), but it differs in that there is no quadratic term that saturates the biasing relation at high mass densities. Little & Weinberg (1994) have compared the influence of density-threshold bias and Cen-Ostriker bias on the void probability function, showing that the size of empty voids is substantially larger for threshold bias at fixed b_σ . MPH98 included Cen-Ostriker bias in their general study of Eulerian bias schemes, and CHWF98 employ both density-threshold bias and power-law bias in their mock catalogs of the 2dF and SDSS redshift surveys.

3.2.3. Sheet bias

The two biasing schemes described above choose galaxies with a probability that is some function of the local mass density alone. In principle, we could envisage other local properties that can influence the efficiency of galaxy formation. Redshift surveys of the local universe reveal a striking pattern in the galaxy distribution, with a large number of galaxies lying in thin walls and narrow filaments on the periphery of huge voids (de Lapparent, Huchra & Geller 1986). The process of gravitational condensation and cooling could be substantially different in a structure that is effectively 2-dimensional rather than 3-dimensional (e.g., Ostriker & Cowie 1981; Vishniac, Ostriker, & Bertschinger 1985; White & Ostriker 1990). These considerations, and the desire to investigate a radical alternative to density-based models, motivate us to consider a biasing scheme in which the efficiency of galaxy formation depends solely on the geometry of the local mass distribution.

In order to identify sheet-like regions of the mass distribution, we compute the three eigenvalues $\lambda_3 > \lambda_2 > \lambda_1$ of the moment of inertia tensor in the $4h^{-1}$ Mpc sphere surrounding each N-body particle. The selection probability for a particle to be a galaxy is

$$P = \begin{cases} A & \text{if } \lambda_3/\lambda_1 \geq B \\ 0 & \text{if } \lambda_3/\lambda_1 < B. \end{cases} \quad (8)$$

This procedure selects galaxies in regions where the mass distribution is planar, $\lambda_3 \gg \lambda_1$, and avoids regions where the mass distribution is isotropic, $\lambda_3 \approx \lambda_1$. The flatness ratio λ_3/λ_1 is correlated with the mass density, so raising the threshold B increases the bias factor b_σ . We choose the value of B so that $b_\sigma(12h^{-1} \text{ Mpc}) = 2$ and the value of A so that $n_g = 0.01h^3 \text{ Mpc}^{-3}$. Because the density and the flatness ratio are not perfectly correlated, the sheet bias scheme differs significantly from the density-threshold bias scheme. In fact, one cannot obtain an arbitrarily high

bias simply by raising the value of B in equation (8), but for our adopted parameters we find that we can always achieve $b_\sigma = 2$. We eliminate all particles that have fewer than 18 neighbors within $4h^{-1}$ Mpc ($\rho_m/\bar{\rho}_m < 0.55$) because the moment-of-inertia tensor would be too noisy.

3.2.4. Pressure and filament bias

We also investigated two other local biasing schemes considered by Weinberg (1995). The first of these, pressure bias, is similar to density-threshold bias, except that the galaxies are selected based on a threshold in $\rho_m\sigma_v^2$ rather than ρ_m , where σ_v^2 is the velocity dispersion in a $4h^{-1}$ Mpc sphere. This scheme is motivated by the possibility that the pressure of the local intergalactic medium could play a role in stimulating galaxy formation. However, the velocity dispersion σ_v^2 is itself fairly well correlated with ρ_m , and we decided to omit results for the pressure bias model from our figures below because they are nearly identical to those of the density-threshold bias model (as also found by Weinberg 1995). This similarity of results seems somewhat at odds with Blanton et al.’s (1998) finding that the inclusion of gas temperature or dark matter velocity dispersion as a variable in the bias relation increases the scale-dependence of the bias factor. We return to this issue in §4.

The second additional scheme, filament bias, is similar to sheet bias (eq. [8]), except that the selection is based on the eigenvalue ratio λ_3/λ_2 instead of λ_3/λ_1 . Our quantitative results for filament bias are somewhat different from those of sheet bias, but they are similar enough that we decided not to include them as separate curves or panels in our figures. In the case of an identical threshold flatness ratio B , the particles selected by filament bias are a subset of those selected by sheet bias. However, a given value of B produces different values of b_σ for sheet and filament bias.

3.3. Non-local Biasing Schemes

In addition to the local biasing schemes described in §3.2, we will investigate two non-local biasing schemes, inspired by the models of Babul & White (1991, hereafter BW91) and Bower et al. (1993, hereafter BCFW93). These papers were a response to measurements of angular clustering in the APM galaxy catalog (Maddox et al. 1990), which showed that the “standard” CDM model (SCDM, with $\Omega = 1$, $h = 0.5$, $n = 1$) predicted the wrong power spectrum shape on large scales. BW91 showed that the SCDM power spectrum could be reconciled with the APM measurements if the formation of luminous galaxies was suppressed in randomly placed spheres with a filling factor $f \sim 0.7$ and radii $R \sim 15h^{-1}$ Mpc, perhaps because of photoionization by quasars (Dekel & Rees 1987; Braun, Dekel, & Shapiro 1988). BCFW93 achieved a similar result with a scheme that modulates galaxy luminosities less drastically but over larger scales (*Gaussian* filter radii $R \sim 20h^{-1}$ Mpc). Both papers argue that the discrepancy between SCDM and the APM data could arise from galaxy formation physics rather than a fundamental failing

of the cosmological model. However, while both papers introduced non-local bias models, neither addressed the question of whether non-locality was essential to achieving the desired modulation of the large scale galaxy correlation function. Subsequent analytic arguments have suggested that non-locality is indeed essential (Coles 1993; Fry & Gaztañaga 1993; Gaztanaga & Baugh 1998; Scherrer & Weinberg 1998), and our results below will strengthen the case.

In our first scheme, which we will refer to simply as “non-local bias,” we select galaxies with a probability

$$P_{\text{nl}} = P_l(1 + \kappa\bar{v}), \quad (9)$$

where P_{nl} and P_l refer respectively to the probability of selecting a mass particle to be a galaxy in the presence and absence of non-local effects. We model the local probability P_l using the power-law scheme described in §3.2.2. We fix the index of this power law, B , by requiring that $b_\sigma = 2$ on a scale of $12h^{-1}$ Mpc and the probability A so that $n_g = 0.01h^3\text{Mpc}^{-3}$. The non-locality is introduced through the dependence of P_{nl} on \bar{v} , which is the density in a top hat sphere of radius R_{nl} about the particle, in units of the rms mass fluctuation on this scale. The large scale smoothing radius R_{nl} defines the scale of the non-local influence, and the modulation coefficient κ controls its strength. Here, we choose $R_{\text{nl}} = 30h^{-1}$ Mpc and $\kappa = 0.25$ for purely illustrational purposes, guided mainly by the fact that non-local effects on this scale can reconcile the SCDM model with the APM correlation function (BCFW93; note our use of a top hat filter rather than a Gaussian filter). While the non-local biasing scheme resembles BCFW93’s cooperative galaxy formation model, our implementation is quite different in detail — Eulerian instead of Lagrangian, with power-law bias taking the place of high peak bias.

In our second non-local scheme, which we will refer to as “void bias,” we randomly place spheres of radius $R_v = 15h^{-1}$ Mpc and eliminate all particles lying within these spheres. We randomly select galaxies from the remaining particles so that $n_g = 0.01h^3\text{Mpc}^{-3}$. We choose the filling factor of the voids so that $b_\sigma = 2$ at $R = 12h^{-1}$ Mpc. This model is similar to that of BW91, who suggested that the voids might be produced by photoionization of pre-galactic gas by quasars.

Although one could easily construct many other non-local bias prescriptions, these two models will suffice to illustrate the differing effects of local and non-local bias. We regard non-local bias as *a priori* less plausible than local bias because of the difficulty of producing coherent modulations in galaxy properties over such large scales. A wide-ranging exploration of non-local models therefore seems justified only if future observational developments force us to consider them more seriously.

3.4. Galaxy Distributions

Figure 4 shows the mass distribution (in panel a) and the various biased galaxy distributions from one of our simulations. We plot the locations of all the galaxy particles that lie in a region $20h^{-1}$ Mpc thick about the center of the cube. The galaxy distributions appear strikingly different from each other even though all of them have the same bias factor $b_\sigma = 2$ at $R = 12h^{-1}$ Mpc.

Density-threshold bias (panel b) completely eliminates galaxies in the low density regions, leaving only the peaks and filaments of the mass distribution populated by galaxies. The power-law bias distribution (panel c) looks like a more dynamically evolved version of the mass distribution, as the contrast between the overdense and the underdense regions is enhanced. However, the underdense regions are not completely devoid of galaxies as they are in the threshold bias model. The sheet bias scheme (panel d) preferentially selects galaxies lying in anisotropic structures, avoiding both the underdense regions and the more isotropic clusters that are so prominent in the power-law model. In this two-dimensional representation, the galaxies appear to lie on thin elongated filaments, with very few knot-like features. The galaxy distribution of the non-local bias model (panel e) looks remarkably similar to that of the local power-law bias model, although they have very different large scale clustering properties as we will see below. The void bias scheme (panel f) completely wipes out all galaxies in some regions. The void radius R_v imprints an obvious characteristic length scale on the galaxy distribution.

3.5. Correlation Function and Power Spectrum

Figure 5 shows the correlation functions $\xi(r)$ and the bias functions $b_\xi(r)$ of the different galaxy distributions under the local biasing schemes. Our normalization condition $\sigma_g(12h^{-1} \text{ Mpc}) = 2\sigma_m(12h^{-1} \text{ Mpc})$ imposes an integral constraint on $\xi_g(r)$ that is, approximately, $\int_0^{12} r^2 \xi(r) dr = \text{constant}$. The bias models that produce higher $\xi(r)$ on small scales must therefore compensate with lower $\xi(r)$ on large scales. However, in all three cases, the correlation bias function $b_\xi(r)$ becomes independent of scale for $r > 8h^{-1} \text{ Mpc}$, and for the two density-based schemes $b_\xi(r)$ is nearly scale-independent for $r > 5h^{-1} \text{ Mpc}$. As noted in §3.2, results for a pressure-threshold bias are similar to those for density-threshold bias, and results for filament bias are similar to those for sheet bias. We also found scale-independent large scale amplification of $\xi(r)$ for the morphology-density relation (Figure 2), which is itself a form of local bias.

Our results for the density-based bias schemes are as expected in light of the analytic argument by Scherrer & Weinberg (1998), which shows that $b_\xi(r)$ tends to a constant in the limit $\xi(r) \ll 1$ for any local density bias applied to a field with a hierarchical clustering pattern. At least in the examples we have examined, the condition $\xi(r) < 1$ seems to be sufficient to reach the asymptotic regime. More importantly, we find the same asymptotically constant behavior of $b_\xi(r)$ for sheet, pressure, and filament bias, where the galaxy density is not a simple function of the mass density. While we cannot examine all conceivable local bias schemes in a finite set of numerical experiments, the combination of our results with the general analytic arguments for local density schemes strongly suggests that scale-independent bias in the regime $\xi(r) < 1$ is a generic property of all local models of galaxy formation.

Figure 6 shows correlation functions and bias functions in the same format as Figure 5, but for the two non-local biasing schemes described in §3.3, “non-local bias” and “void bias.” We also show the results of the local power-law biasing scheme (from Figure 5) for comparison. The

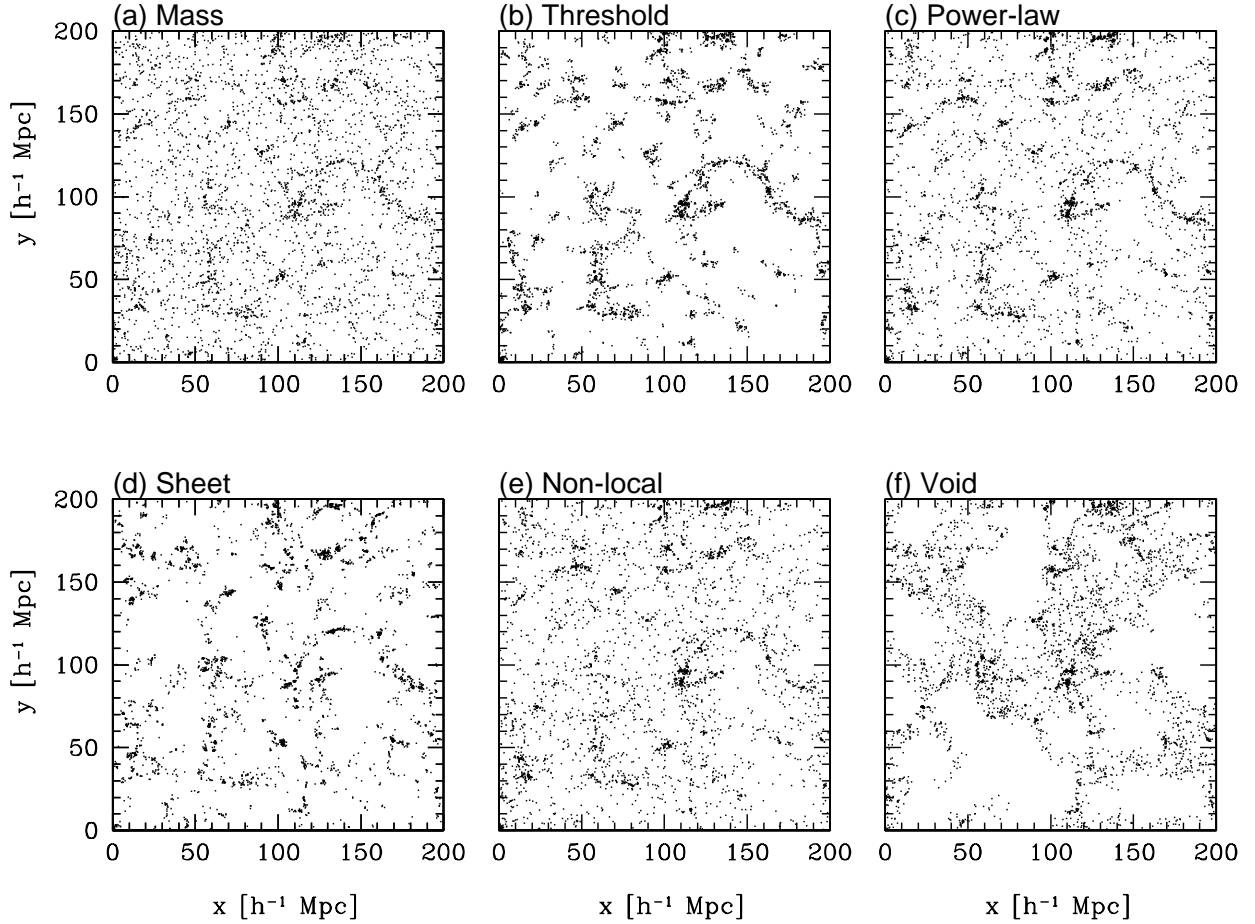


Fig. 4.— Galaxy distributions under the different biasing schemes. The panels show the galaxy distributions in a slice $20h^{-1}\text{Mpc}$ thick and spanning $200h^{-1}\text{Mpc}$ in the other two dimensions. (a) Underlying mass distribution, randomly sampled to $n_g = 0.01h^3\text{Mpc}^{-3}$. The remaining panels show the galaxy distributions under (b) density-threshold bias, (c) power-law bias, (d) sheet bias, (e) non-local bias, and (f) void bias.

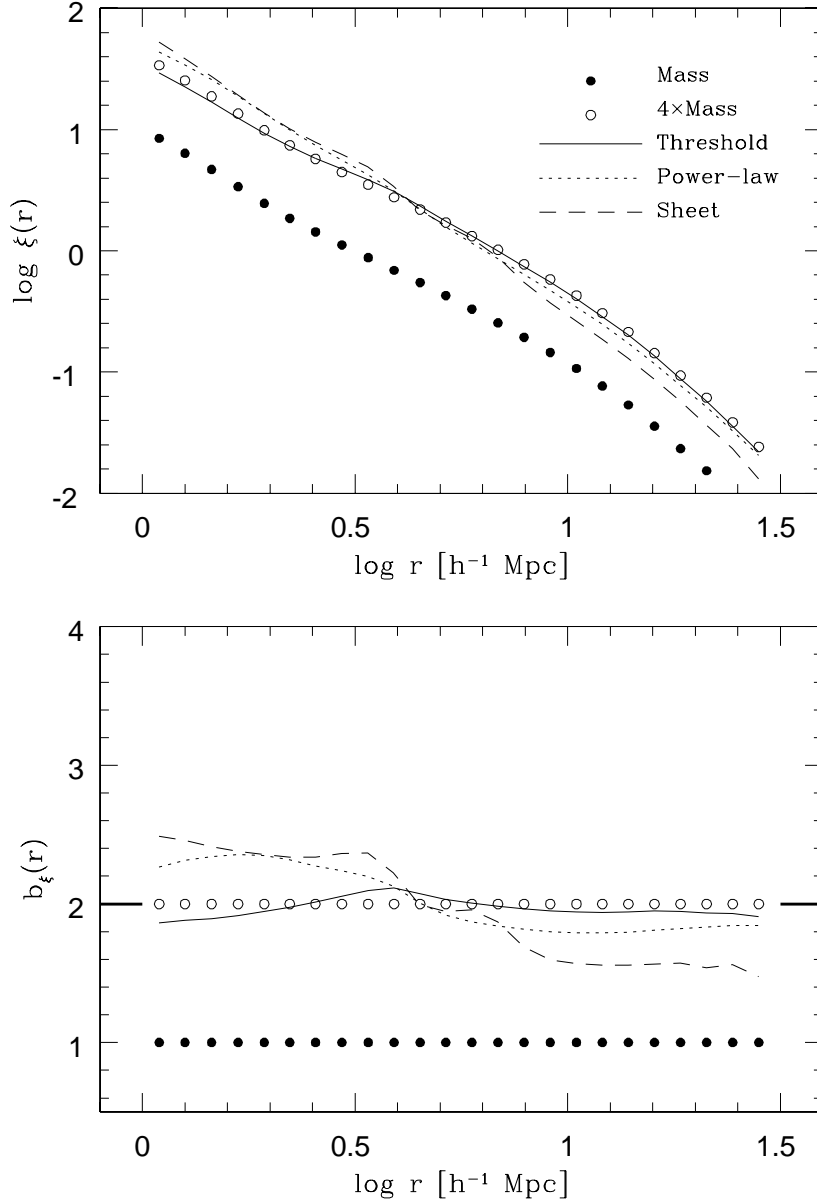


Fig. 5.— Top: Correlation functions of the galaxy distributions under the different local biasing schemes: density-threshold bias (solid), power-law bias (dotted), and sheet bias (dashed). Filled circles show the mass correlation function, and open circles show the mass correlation function multiplied by $b_\sigma^2(12h^{-1} \text{ Mpc}) = 4$. Bottom: The bias functions $b_\xi(r)$ defined in equation (3).

non-local bias scheme clearly leads to enhanced clustering on scales larger than about $10h^{-1}$ Mpc. The bias function increases monotonically up to the largest scale shown in the Figure, growing by almost a factor of two between $10h^{-1}$ Mpc and $30h^{-1}$ Mpc. Void bias boosts the correlation function substantially on scales $r \sim R_v \sim 15h^{-1}$ Mpc, while at larger scales the imprint of empty regions with a characteristic diameter causes $\xi(r)$ to turn over rapidly. Our results confirm the arguments of BW91 and BCFW93 that large scale modulations of galaxy formation can alter the shape of $\xi(r)$ enough to reconcile a standard CDM mass correlation function with the APM galaxy correlation function. However, the results in Figure 5 imply that non-locality is not an incidental feature of the BW91 and BCFW93 models but is essential to obtaining a scale-dependent $b_\xi(r)$ at large r .

Figure 7 shows the power spectra $P(k)$ and the Fourier space bias functions $b_P(k)$ for the local biasing schemes. The arrows marked $k_8 = 2\pi/(2 \times 8) = 0.3927h \text{ Mpc}^{-1}$ and $k_{12} = 2\pi/(2 \times 12) = 0.2618h \text{ Mpc}^{-1}$ represent the wavenumbers corresponding to the length scales $8h^{-1}$ Mpc and $12h^{-1}$ Mpc, at which we normalize the amplitude of the mass power spectrum and the bias factor, respectively. This bias function $b_P(k)$ is also independent of scale on large scales, where it is approximately equal to $b_\sigma(12h^{-1} \text{ Mpc}) = 2$. This Figure quantifies clustering on scales up to the fundamental wavelength of our $400h^{-1}$ Mpc simulation cube, well beyond those probed by the correlation functions in Figure 5. The constancy of $b_P(k)$ at small k reinforces our conclusion that the bias functions of local biasing schemes remain scale-independent on *all* large scales. The bias functions become truly scale-independent only for $k < k_s = 0.2h \text{ Mpc}^{-1}$ [corresponding to length scales $R > 2\pi/(2 \times k_s) \approx 15h^{-1}$ Mpc], although our binning in Fourier space at the low wavenumbers is admittedly coarse. This value of k_s is comparable to the fundamental frequency of the simulation box used by MPH98, who found a mild, monotonic scale-dependence of $b_P(k)$ on smaller scales ($k > 0.1h \text{ Mpc}^{-1}$).

Figure 8 shows the power spectra and the bias functions for the non-local and void biasing schemes, again with the local power-law results shown for comparison. The arrow marked $k_{30} = 2\pi/(2 \times 30) = 0.1047h \text{ Mpc}^{-1}$ represents the wavenumber corresponding to $30h^{-1}$ Mpc, the scale of influence in the non-local model. The power spectrum of the non-local model shows strong curvature at roughly this scale and dramatically enhanced amplitude on larger scales. The bias function $b_P(k)$ increases with scale and does not settle to a constant even near the largest scales shown, the fundamental frequency of the cubical simulation box. The void bias model once again exhibits a characteristic feature at the scale of the voids, corresponding to the wavenumber $k_v = 2\pi/(2 \times R_v) = 0.2094h \text{ Mpc}^{-1}$, with a large difference in $b_P(k)$ on either side of it. The non-local and the void bias schemes can both enhance the amplitude and change the shape of the underlying mass power spectrum, even on very large scales.

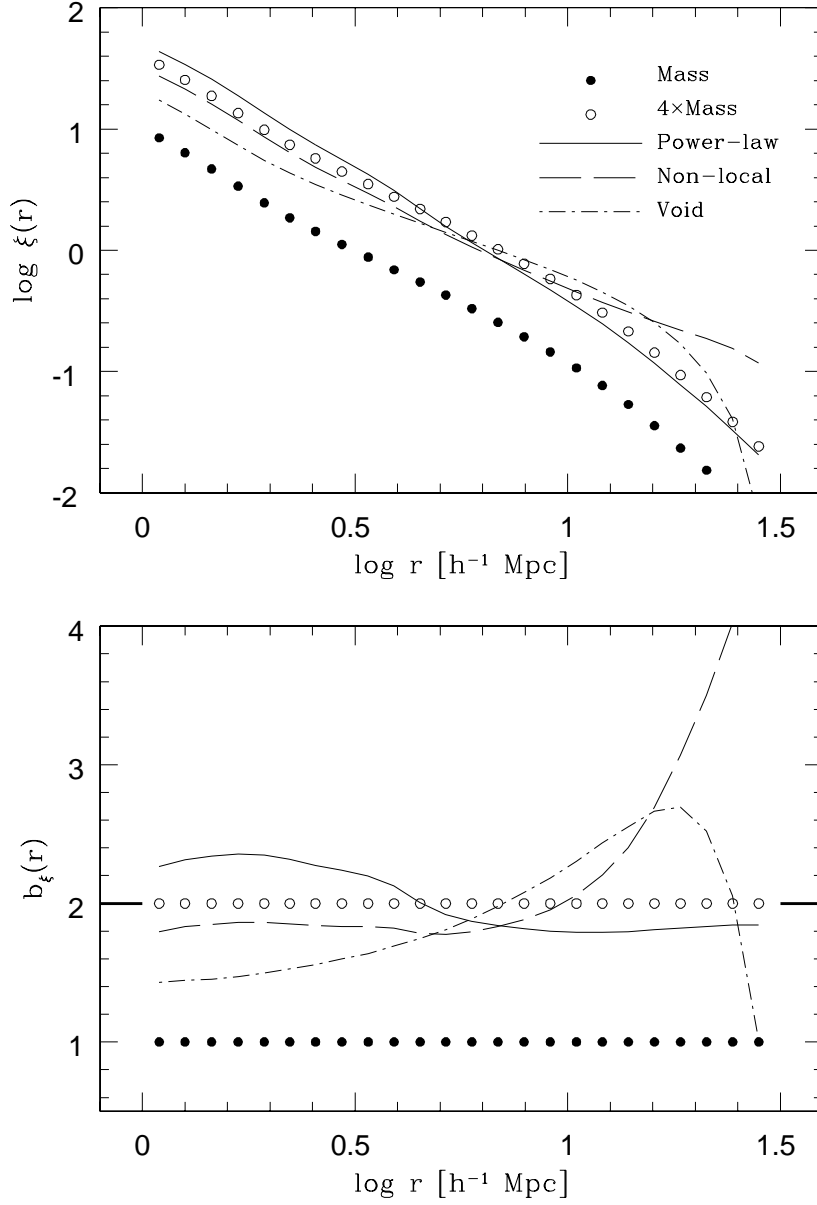


Fig. 6.— Top: Correlation functions of the galaxy distributions under the power-law (solid), non-local (long-dashed), and void (dot-dashed) biasing schemes. Bottom: The bias functions $b_\xi(r)$ defined in equation (3).

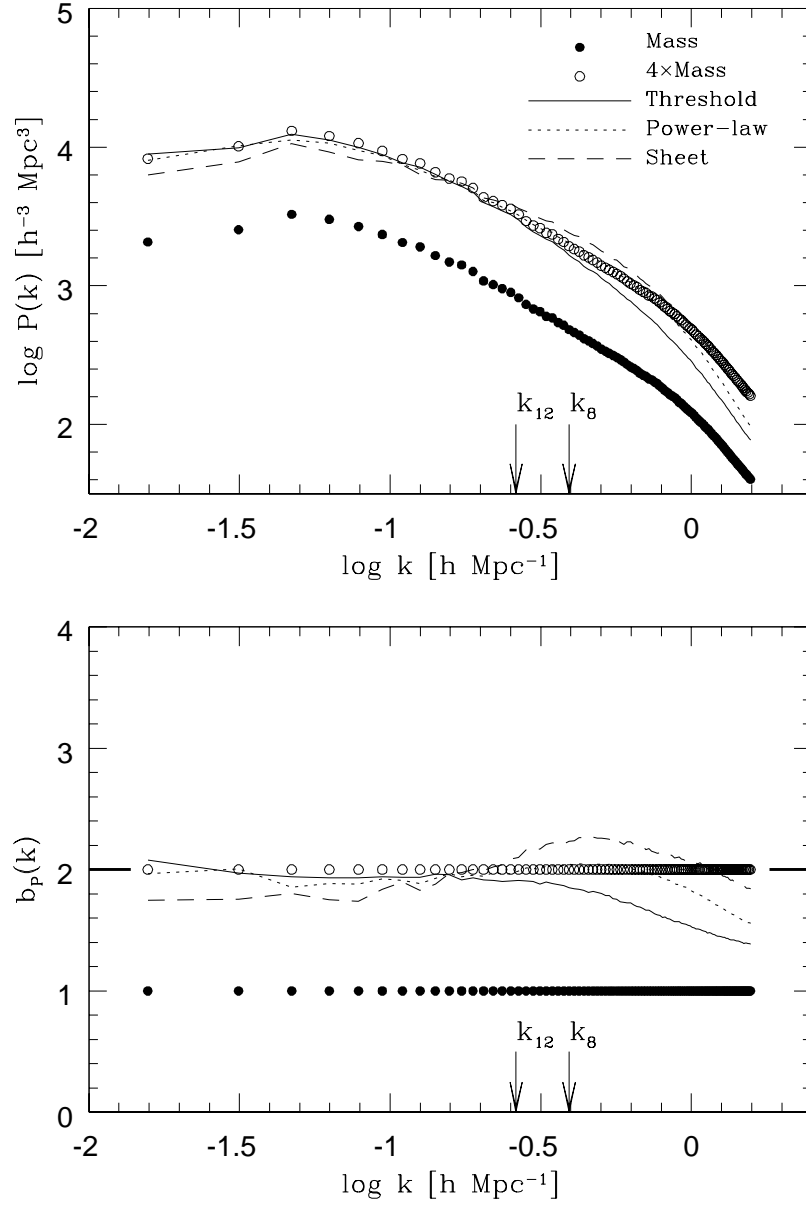


Fig. 7.— Top: Power spectra of the galaxy distributions under the different local biasing schemes. Bottom: The bias functions $b_P(k)$ defined in equation (4).

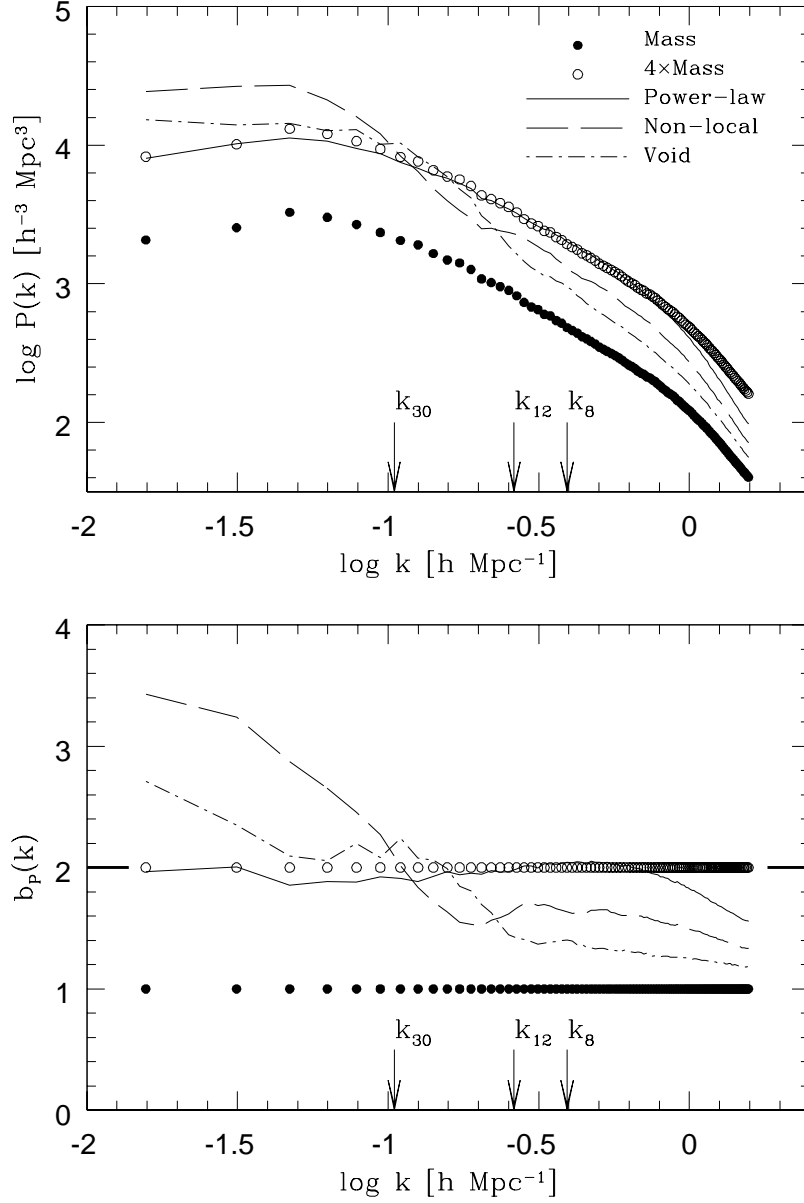


Fig. 8.— Top: Power spectra of the galaxy distributions under the power-law, non-local, and void biasing schemes. Bottom: The bias functions $b_P(k)$ defined in equation (4).

3.6. Higher-Order Moments

The correlation function and power spectrum measure second moments of the galaxy distribution as a function of scale. We now turn to some of the simplest measures of higher-order clustering, the hierarchical amplitudes

$$S_J(R) \equiv \frac{\langle \delta^J \rangle_c}{\langle \delta^2 \rangle^{J-1}}, \quad (10)$$

where $\langle \delta^J \rangle_c$ and $\langle \delta^2 \rangle$ are the J -th connected moment and the variance, respectively, of the density contrast field smoothed with a top hat filter of radius R . The third and fourth connected moments are $\langle \delta^3 \rangle$ and $\langle \delta^4 \rangle - 3\langle \delta^2 \rangle^2$, respectively. For Gaussian initial conditions, $(J - 1)$ -th order gravitational perturbation theory predicts that $S_J(R)$ is independent of the amplitude of $P(k)$, independent of R for a power-law $P(k)$, and only weakly dependent on R (i.e., varying much more slowly than $\langle \delta^J \rangle_c$) for a more general $P(k)$ (Fry 1984; Juszkiewicz, Bouchet, & Colombi 1993; Bernardeau 1994). A local linear or non-linear transformation of the smoothed field $\delta(\mathbf{x})$ — i.e., a form of local bias applied on scale R — alters the values of S_J , but it does not destroy this hierarchical behavior (Fry & Gaztañaga 1993). The values of S_J can therefore provide a diagnostic for the properties of the biasing relation. The hierarchical behavior of moments of the observed IRAS and optical galaxy distributions (e.g., Meiksin, Szapudi & Szalay 1992; Bouchet et al. 1993; Gaztañaga 1992, 1994; Kim & Strauss 1998) supports the hypothesis of Gaussian initial conditions, and it has also been used as an argument against non-local bias (Frieman & Gaztañaga 1994).

Figure 9 shows the rms fluctuation $\sigma \equiv \langle \delta^2 \rangle^{1/2}$ of the mass and galaxy density fields as a function of the top hat smoothing radius R_{th} . For the sake of clarity, we show error bars only for the mass distribution; error bars for the galaxy distributions are similar. We compute the statistical errors as the dispersion in the measurements from four independent simulations, divided by $\sqrt{3}$. Our normalization condition, $b_\sigma(12) = 2$, forces the rms fluctuations of all models to be equal at $R_{\text{th}} = 12h^{-1}$ Mpc. In Figures 10 and 11, we plot the hierarchical amplitudes S_3 and S_4 as a function of $\log \sigma$, which can be related to a top hat filter radius using Figure 9. We compute all moments by CIC-binning the mass or galaxy distributions onto a 200^3 grid and smoothing this density field with top hat filters of successively larger radii.

Solid lines in Figure 10 show S_3 for the various bias models, with error bars estimated from the dispersion of S_3 values measured from the four independent simulations, divided by $\sqrt{3}$. The filled circles are the same in all the panels and show the values of S_3 predicted by perturbation theory for the underlying mass distribution, computed for our tilted CDM power spectrum using the equations in §3.5 of Bernardeau (1994). The predictions agree very well with the values measured from the underlying mass distribution (panel a), demonstrating that the scale dependence of S_3 of the mass distribution can be reproduced quite accurately using perturbation theory if the matter power spectrum is known *a priori*. This Figure also shows that the finite size of the simulation box leads to unreliable estimates of S_3 for $\log \sigma_g \lesssim -0.8$, corresponding to $R_{\text{th}} \approx 45h^{-1}$ Mpc.

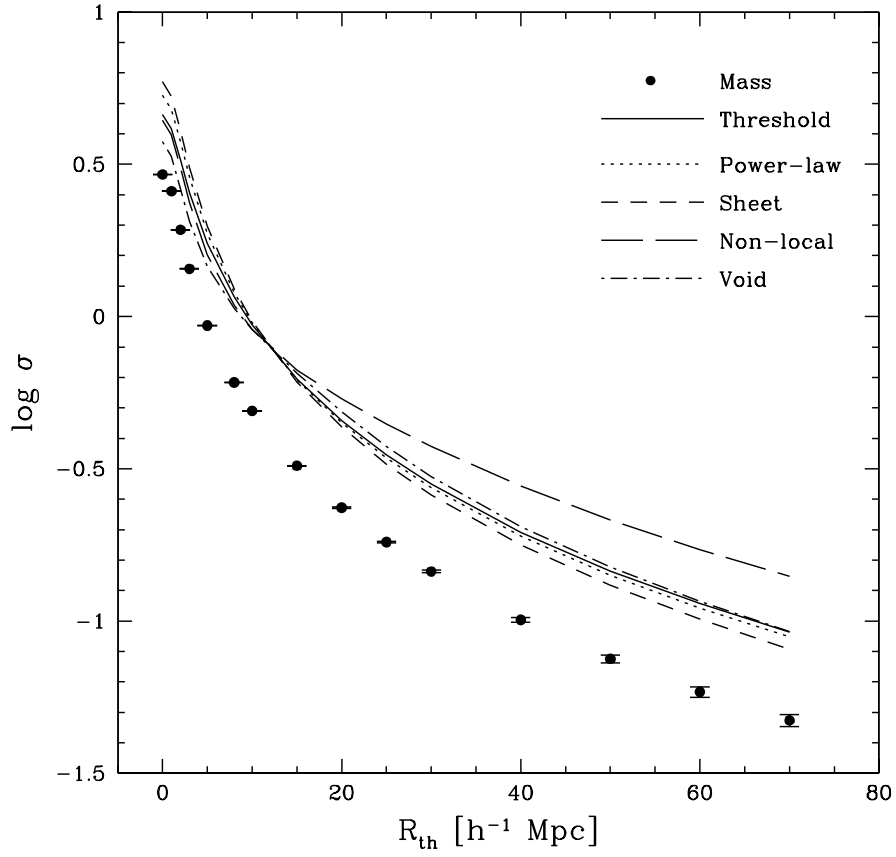


Fig. 9.— The rms fluctuation amplitude σ as a function of the radius R_{th} of the top hat filter used to smooth the density fields. The solid circles show the σ of the mass distribution, while the lines represent the various biased galaxy density fields. The error bars show the 1σ deviation computed as the dispersion in the measurements from four independent simulations and divided by $\sqrt{3}$.

A linear bias $\delta_g = b\delta$ would reduce the amplitude of S_3 by a factor of b on all scales. Our bias models, both local and non-local, have a more complicated effect, altering the scale-dependence of S_3 . Density-threshold and sheet bias (panels b and d) significantly reduce the amplitude of S_3 on all scales, and for density-threshold bias S_3 becomes almost scale-independent over the range $0.1 < \sigma < 1$. The high weight assigned to dense regions boosts the value of S_3 on small scales in the power-law bias model (panel c), though in the range $0.1 < \sigma < 1$ this model tracks the behavior of the mass distribution remarkably closely. Values of $S_3(\sigma)$ for the non-local bias model (panel e) are similar to those for the local power-law bias. Finally, void bias (panel f) produces a systematically lower $S_3(\sigma)$ and a feature at $\sigma = 0.25$, corresponding to a physical scale close to the diameter of the voids.

Figure 11 shows $S_4(\sigma)$ in the same format as Figure 10. The perturbation theory predictions, based on the equations of Bernardeau (1994), again accurately match the values measured from the mass distribution over the range $0.1 < \sigma < 1$. Linear bias would decrease S_4 by a factor of b^2 on all scales. The relative behavior of $S_4(\sigma)$ for the different biasing schemes is similar to that of $S_3(\sigma)$. Thus, density-threshold bias reduces both the amplitude and the scale-dependence of S_4 , while sheet bias primarily reduces its amplitude. The power-law and the non-local biasing schemes preserve the S_4 of the mass distribution over the range $0.1 < \sigma < 1$ and depart drastically from it outside this range. Void bias once again produces a break at $\sigma \approx 0.25$. Note that although Figures 10 and 11 demonstrate the scale-dependence of S_3 and S_4 , all of our biasing models (even the non-local and void bias) still preserve the basic hierarchical pattern of moments predicted by gravitational perturbation theory with Gaussian initial conditions; for example, the ratios S_3 and S_4 change by less (usually much less) than a factor of two between $\log \sigma = -0.5$ and $\log \sigma = 0$, even though the denominators σ^4 and σ^6 change by factors of 100 and 1000, respectively.

Our results provide two cautionary notes for efforts to infer the bias relation from measurements of hierarchical amplitudes. First, the agreement between observed amplitudes and those predicted for the mass distribution has been used to argue that galaxy formation is unbiased (e.g., Gaztañaga 1994). However, we find that the power-law bias model, which is not particularly contrived, happens to yield nearly the same results as the mass distribution, at least for S_3 and S_4 . Second, the agreement of $S_3(\sigma)$ and $S_4(\sigma)$ with perturbation theory predictions has been used to argue against the BCFW93 cooperative galaxy formation bias model (Frieman & Gaztañaga 1994). However, the non-local model adopted here gives $S_3(\sigma)$ and $S_4(\sigma)$ results similar to those of the local power-law bias model (and the mass distribution), suggesting that the failure of the BCFW93 model may not extend generally to all similar non-local models.

3.7. Quadratic Bias Parameters

Ratios of the moments of galaxy counts can also be interpreted in terms of a hierarchy of bias parameters describing the relation between galaxies and mass (Fry & Gaztañaga 1993; Juszkiewicz et al. 1995). Suppose that there is a relation $\delta_g = f(\delta_m)$ between the galaxy and mass density

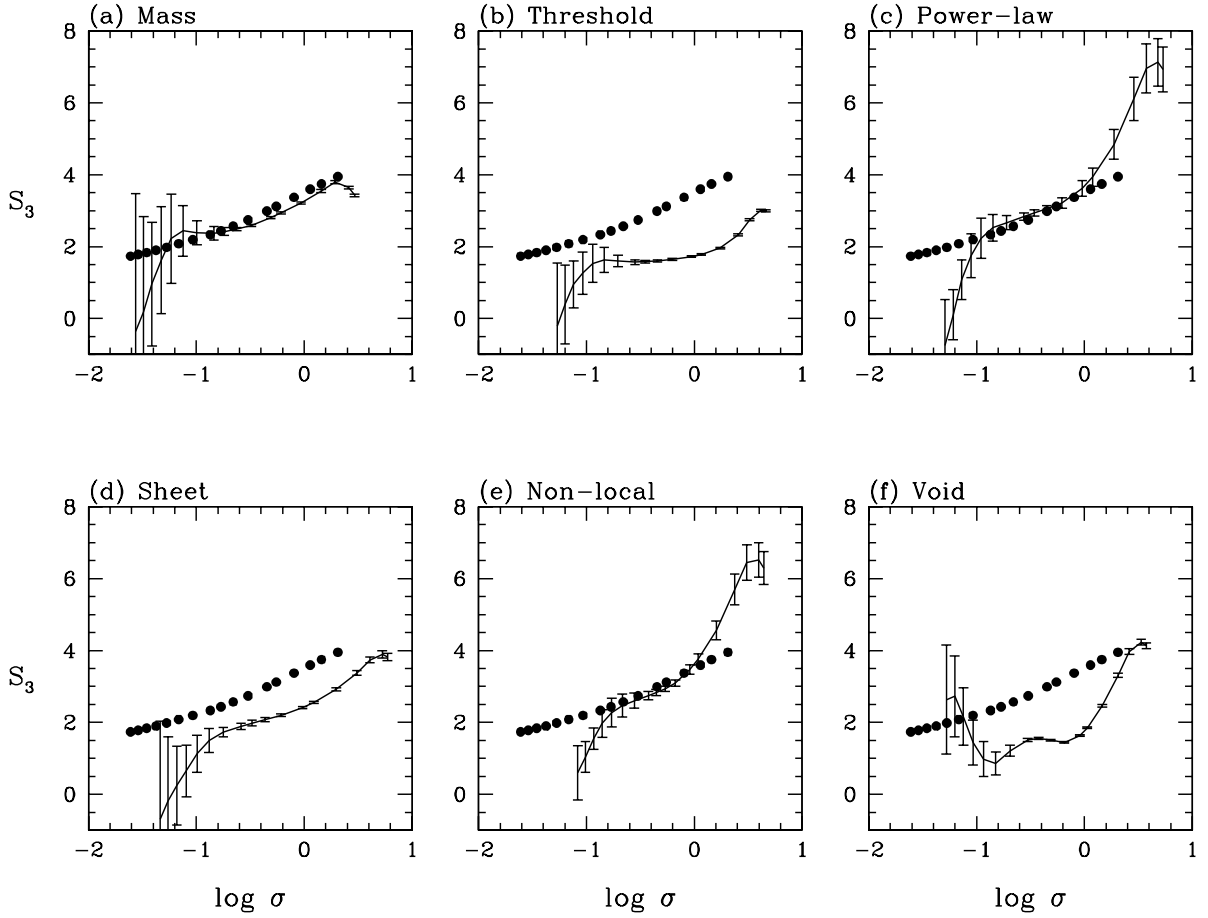


Fig. 10.— The hierarchical amplitude S_3 as a function of the rms density fluctuation amplitude σ for the mass and biased galaxy distributions. Solid circles show $S_3(\sigma)$ predicted by perturbation theory for the underlying mass density field. Error bars show the 1σ uncertainty computed as the dispersion in the measurements from four independent simulations divided by $\sqrt{3}$.

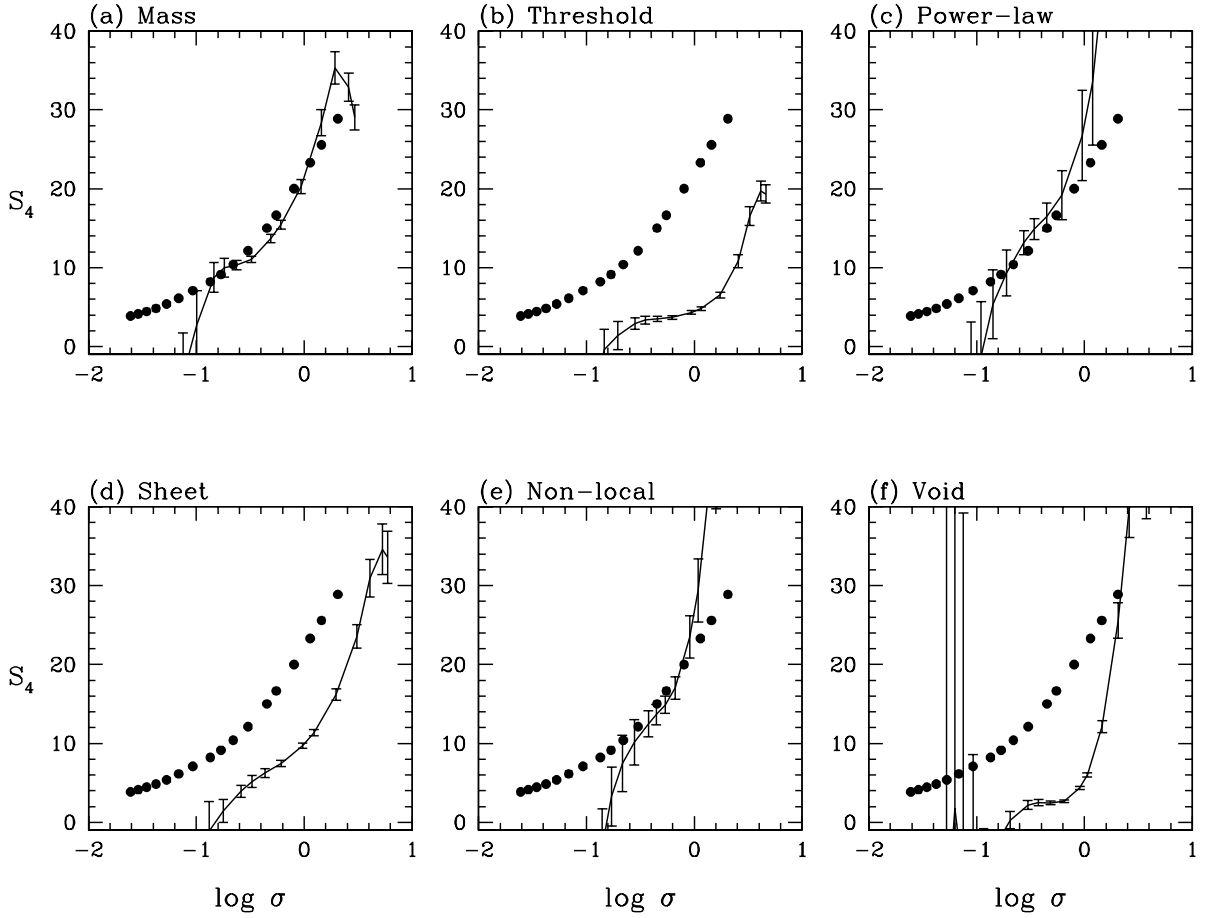


Fig. 11.— The hierarchical amplitude S_4 as a function of the rms density fluctuation amplitude σ for the mass and biased galaxy distributions. Solid circles show $S_4(\sigma)$ predicted by perturbation theory for the underlying mass density field. Error bars show the 1σ uncertainty computed as the dispersion in the measurements from four independent simulations divided by $\sqrt{3}$.

contrast fields after both are smoothed over scale R . In the limit of small amplitude fluctuations, $|\delta_m| \ll 1$, the function $f(\delta_m)$ can be approximated by a second-order Taylor expansion,

$$\delta_g \equiv f(\delta_m) \simeq b_1 \delta_m + \frac{1}{2} b_2 \delta_m^2 - \frac{1}{2} b_2 \sigma_m^2, \quad (11)$$

where the third term ensures that $\langle \delta_g \rangle = 0$. The “linear” bias parameter b_1 gives the slope of the galaxy-mass relation, and in the limit of first-order perturbation theory it is equal to other bias parameters such as b_σ and b_ξ . The Taylor expansion (11) can be regarded as the justification for adopting the linear bias model for some calculations in the limit of small δ_m . However, the hierarchical amplitude S_3 is only non-zero in second-order perturbation theory, so to compute the effect of bias on S_3 one must use the full second-order expansion (11) even in the small- δ_m limit. The result is (Fry & Gaztañaga 1993; Juszkiewicz et al. 1995)

$$S_{3g} = \frac{S_{3m}}{b_1} + \frac{3b_2}{b_1^2}. \quad (12)$$

At the same order, the variance of the galaxy density is (R. Scoccimarro, private communication)

$$\sigma_g^2 = b_1^2 \sigma_m^2 + S_{3m} b_1 b_2 \sigma_m^4 + \frac{1}{2} b_2^2 \sigma_m^4. \quad (13)$$

In general, there will be some scatter about the relation $\delta_g = f(\delta_m)$, and even if the scatter is small at one scale it could be large at another scale. We will return to this issue in §3.9 below. For now, however, we investigate the behavior of the linear and quadratic bias parameters b_1 and b_2 defined as the simultaneous solutions to equations (12) and (13). The thick and the thin dashed lines in Figure 12 plot these parameters as a function of R_{th} , the radius of the top hat filter used to define the smoothed density fields. The thick and thin solid lines show the results of an alternative definition in which equation (13) is replaced by the first-order relation $b_1 = b_\sigma = \sigma_g / \sigma_m$ (eq. [5]). The two definitions are identical in the limit $\sigma_m \ll 1$, since the σ_m^4 terms in equation (13) become negligible. We estimate the errors in b_2 as the dispersion in the values derived from the four independent simulations, divided by $\sqrt{3}$. The errors in b_1 are tiny over the range of scales considered, so we do not show them in the Figure.

The rms fluctuation σ is given by an integral of $\xi(r)$. Since we have already shown that $b_\xi(r)$ tends to a constant on large scales in local bias models, we expect b_1 to become constant on large scales in local models as well. This is just the behavior that we find in Figure 12, though in the sheet bias model there is scale-dependence out to $R \sim 15h^{-1}$ Mpc. The void bias model has a more scale-dependent value of b_1 , though it still settles to $b_1 = 2$ for $R \geq 20h^{-1}$ Mpc. In the non-local model, on the other hand, b_1 increases monotonically with scale up to the largest scales plotted, reaching $b_1 = 3$ at $R_{\text{th}} = 70h^{-1}$ Mpc. In all cases the definition $b_1 = b_\sigma$ is less scale-dependent than the definition from simultaneous solution of equations (12) and (13).

Given that b_1 and b_ξ become scale-independent on large scales in all of our local biasing models, it is tempting to conjecture that the quadratic bias parameter b_2 also becomes scale-independent

in this regime. Indeed, one might extend this conjecture to scale-independence of the whole hierarchy of non-linear bias parameters defined by Fry & Gaztañaga (1993), which come from the successively higher order terms in the Taylor expansion of $\delta_g = f(\delta_m)$. Unfortunately, the noise in estimates of S_3 in our finite simulation box makes it difficult to test even the b_2 conjecture. The density-threshold and power-law bias results appear marginally consistent with a constant b_2 for $R_{\text{th}} > 15h^{-1}$ Mpc, while the sheet bias model appears marginally inconsistent with constant b_2 . The value of b_2 certainly shows more scale-dependence at large R_{th} in the non-local and void bias models. The value of b_2 is scale-dependent in all models except density-threshold bias for $R_{\text{th}} < 15h^{-1}$ Mpc, which is not too surprising since the Taylor expansion (11) and perturbation theory calculation (12) break down as σ approaches one.

3.8. Pairwise Peculiar Velocities

Gravitational evolution of the inhomogeneous mass distribution induces peculiar velocities on all the mass particles. The pairwise velocity dispersion, which can be estimated from the anisotropy of the redshift-space correlation function $\xi(r_p, \pi)$ of galaxy redshift surveys (Davis & Peebles 1983; Bean et al. 1983), provides a diagnostic of Ω by way of the ‘‘Cosmic Virial Theorem’’ (Peebles 1976). It has also been used as a direct test of cosmological models (e.g., Davis et al. 1985). The first and second moments of the pairwise velocity distribution enter into the BBGKY equations (Davis & Peebles 1977) and analytic calculations of redshift-space distortions of $\xi(r_p, \pi)$ (Fisher 1995 and references therein). However, even if galaxies have the same velocity field as the dark matter, these statistical characterizations of galaxy velocities can be strongly affected by bias because of the pair weighting. For example, if biased galaxy formation preferentially populates dense regions with high velocity dispersions, then the pairwise dispersion of the galaxies will exceed the pairwise dispersion of the mass.

Figure 13 shows the first moment of the pairwise velocity distribution, the mean pairwise radial velocity

$$V_{12}(r) \equiv \langle (\mathbf{v}_1 - \mathbf{v}_2) \cdot \mathbf{r}_{12} \rangle. \quad (14)$$

Here \mathbf{v}_1 and \mathbf{v}_2 are the velocities of two particles separated by the vector \mathbf{r}_{12} , and the angular bracket denotes an average over all particle pairs with separation $r = |\mathbf{r}_{12}|$. Error bars are estimated from the dispersion among the four independent simulations, divided by $\sqrt{3}$. In a linear bias model $\delta_g = b\delta_m$ where the galaxies follow the same velocity field as the mass, $V_{12}^{\text{gal}}(r) = bV_{12}^{\text{mass}}(r)$ in the small δ_m (large r) limit (Fisher et al. 1994). In line with this expectation, all three of our local bias models exhibit a nearly constant amplification of $V_{12}(r)$ for $r > 10h^{-1}$ Mpc, by a factor that is close to the model’s value of $b_\xi(r)$ from Figure 5. At smaller scales, however, the shape of $V_{12}(r)$ depends strongly on the biasing scheme, in particular on the degree to which it weights the densest regions. Thus, the power-law bias model has the highest $V_{12}(r)$ and the sheet model, which avoids the isotropic clusters, has a $V_{12}(r)$ that falls below the mass $V_{12}(r)$ at small separations. The non-local model roughly follows the power-law model on

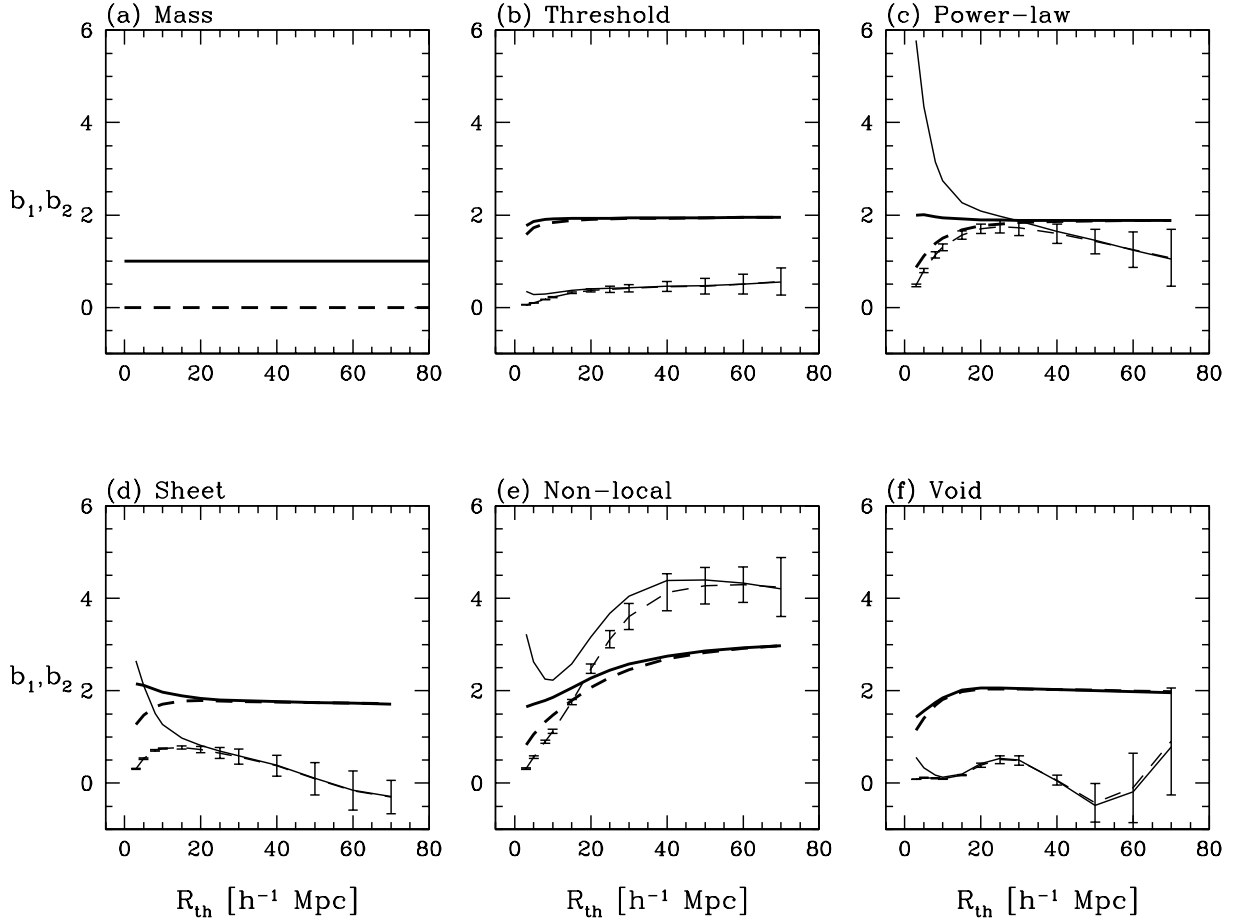


Fig. 12.— The linear and quadratic bias parameters b_1 and b_2 , as a function of the top hat smoothing radius R_{th} . Thick and thin solid lines show $b_1 \equiv b_\sigma$ (eq. [5]) and b_2 computed from equation (12). Thick and thin dashed lines show b_1 and b_2 computed by simultaneously solving equations (12) and (13). The 1σ error bars on b_2 are computed using the dispersion in the measurements from four independent simulations, divided by $\sqrt{3}$.

small scales, and it does not settle to a constant amplification of $V_{12}(r)$ at large scales. The “bias factor” defined by $b_v(r) = V_{12}^{\text{gal}}(r)/V_{12}^{\text{mass}}(r)$ for this model has a scale-dependence at large r that is reminiscent of (but not as strong as) that of $b_\xi(r)$ (Figure 6). The void bias model is perhaps the oddest counterexample to the linear bias expectation: since galaxies are eliminated from randomly placed voids with no regard to their density or velocity, void bias does not alter $V_{12}(r)$ at all. This result emphasizes a difference between the void bias model and our other models, namely that it enhances $\xi(r)$ and $P(k)$ by imprinting an additional, independent clustering pattern on the galaxy distribution rather than by preferentially selecting galaxies in clustered regions.

Figure 14 shows the second moment of the pairwise velocity distribution, the pairwise radial velocity dispersion

$$\sigma_v^2(r) \equiv \langle |(\mathbf{v}_1 - \mathbf{v}_2) \cdot \mathbf{r}_{12}|^2 \rangle - V_{12}^2(r), \quad (15)$$

where the average is again over pairs of separation $r = |\mathbf{r}_{12}|$. Measurements of this quantity from the anisotropy of $\xi(r_p, \pi)$ are sensitive to the presence or absence of rich clusters in the redshift sample (Mo, Jing & Borner 1993; Zurek et al. 1994; Somerville, Primack, & Nolthenius 1997). Figure 14 illustrates another shortcoming of the pairwise velocity dispersion as a cosmological diagnostic: it is sensitive to the details of the biasing scheme, so it cannot be predicted without a fully specified model of biasing. The two models with the steepest small scale correlation functions, sheet bias and power-law bias, have, respectively, the lowest and highest pairwise velocity dispersions at small scales because of the relative weights they assign to rich clusters. The sheet bias model has $\sigma_v^2(r)$ well below the mass $\sigma_v^2(r)$ for $r < 4h^{-1}$ Mpc. At large r , all bias models except for the void model produce an amplification of $\sigma_v^2(r)$, but not by a factor that is simply related to the large scale bias. Because many of the pairs contributing high values of the pairwise velocity at large r have one member in a high-dispersion cluster, the pairwise dispersion statistic is heavily influenced by cluster weighting even at large scales.

Recognizing the sensitivity of the pairwise velocity dispersion to the presence of clusters in redshift surveys and to the nature of bias, Kepner, Summers, & Strauss (1997) and Strauss, Ostriker, & Cen (1998) have proposed alternative statistics that measure the velocity dispersion as a function of the local number density of galaxies instead of averaging over all pairs. (Davis, Miller, & White [1997] and Landy, Szalay, & Broadhurst [1998] have explored other approaches that measure a globally averaged quantity but do not weight by galaxy pairs.) In particular, Kepner et al. (1997) suggested that the slope of the relation between the velocity dispersion and the galaxy number density could provide a diagnostic for Ω . Figure 15 shows $\sigma_v(\rho/\bar{\rho})$, the velocity dispersion as a function of the local galaxy overdensity, with both quantities computed in spheres of radius $3h^{-1}$ Mpc. We also compute the intrinsic dispersion in σ_v at fixed $\rho/\bar{\rho}$, which is shown by the error bars. This measure of $\sigma_v(\rho/\bar{\rho})$ is similar but not identical to the measures proposed by Kepner et al. (1997) and Strauss et al. (1998). Figure 15 shows that the slope of σ_v vs. $\rho/\bar{\rho}$ is systematically lower for biased galaxy distributions than for the underlying mass distribution, as anticipated by Kepner et al. (1997) and Strauss et al. (1998). More significantly, the slope is not simply related to the rms bias on the $3h^{-1}$ Mpc measurement scale (see Figure 9) but depends

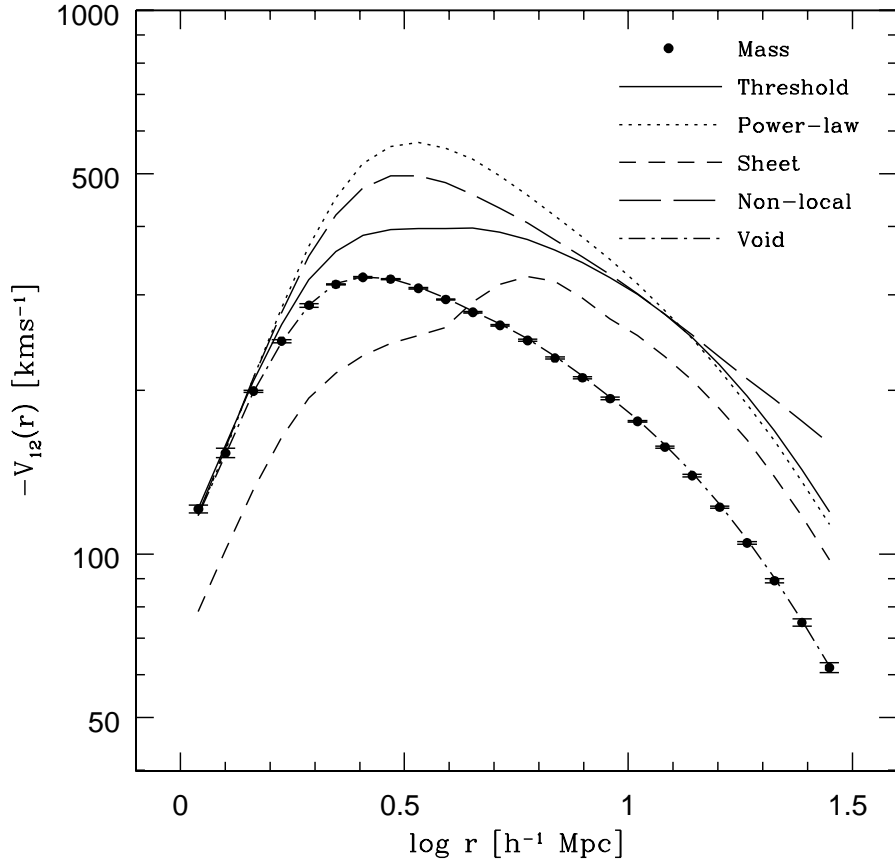


Fig. 13.— The mean pairwise radial peculiar velocity $V_{12}(r)$ as a function of pair separation for the underlying mass distribution and the various biased galaxy distributions. Error bars, usually smaller than the points, are plotted for the mass distribution only; they are similar in magnitude for all the galaxy distributions. We plot V_{12} logarithmically so that a constant offset between galaxy and mass curves corresponds to a constant amplification of $V_{12}(r)$, as expected for linear bias.

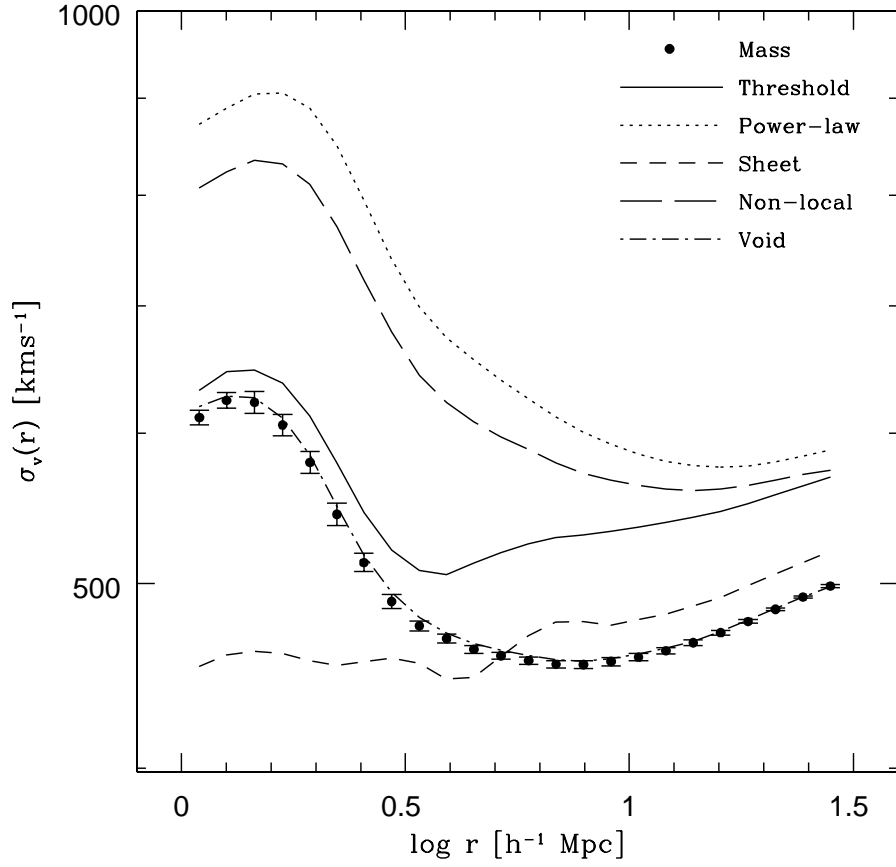


Fig. 14.— The mean pairwise radial peculiar velocity dispersion as a function of the pair separation for the mass and the various biased galaxy distributions. Error bars are shown only for the mass distribution and are similar in magnitude for all the galaxy distributions.

on the details of the adopted biasing scheme. Measuring σ_v as a function of density does soften the extreme sensitivity of the pairwise dispersion to the details of the bias model, but probably not enough to make this statistic a good one with which to measure Ω . Measurements of $\sigma_v(\rho/\bar{\rho})$ can provide a test of cosmological models, but only if the relation between galaxies and mass is reliably specified.

3.9. Galaxy and Mass Density Fields

Any physical biasing of the galaxy distribution can lead to a non-trivial relation between the galaxy and the mass density fields. We have introduced several different definitions of bias factors, each related to a specific statistical measure of clustering. A more general description of the effect of bias is the conditional probability $P(\delta_g|\delta_m)$ of finding galaxy density contrast δ_g where the mass density contrast is δ_m (DL98). This formulation implicitly assumes a smoothing scale on which the fields δ_g and δ_m are defined, and in general both the mean relation and the scatter about it will depend on the smoothing scale.

Figure 16 shows the median and the 10th and 90th percentile limits of the distribution of smoothed galaxy density contrasts δ_g at given values of the smoothed mass density contrast δ_m . The dotted line that runs along the diagonal in each panel shows the relation $\delta_g = 2\delta_m$ expected for linear bias with a constant bias factor $b = 2$. Different rows correspond to different biasing schemes, while the four columns from left to right show results for Gaussian smoothing radii $R_s = 3, 6, 10$ and $15h^{-1}$ Mpc, respectively. We compute the distribution and the different percentile values using the density fields from the four independent simulations.

The effect of the density-threshold bias is remarkably close to linear bias at all smoothing scales and density contrasts, breaking down only where it must at $\delta_g \approx -1$. This result is consistent with the very small values of b_2 found for this model (Figure 12). The median $\delta_g(\delta_m)$ is markedly more non-linear for the power-law model, approaching the dotted line only for a large smoothing length $R_s = 15h^{-1}$ Mpc. The median relation for the sheet model is fairly linear, though always shallower than $\delta_g = 2\delta_m$. The non-local model has a noticeably curved median relation even at $R_s = 15h^{-1}$ Mpc, consistent with the rise in b_2 for this model at large scales (Figure 12). For the void model, the scatter in δ_g at fixed δ_m is so large that the median relation alone provides little information.

More generally, the scatter between δ_g and δ_m reveals the influence of factors other than the local mass density in shaping the galaxy distribution. As one might expect, the scatter about the median relation is small for the bias models based on local mass density (density-threshold and power-law bias), and it decreases rapidly with increasing smoothing. Some scatter is inevitable because of shot noise in the galaxy distribution, and because the density smoothed with a Gaussian filter of radius R_s is not perfectly correlated with the density smoothed with a top hat of radius $R_{\text{th}} = 4h^{-1}$ Mpc (as used in the biasing prescriptions). The influence of large scale density

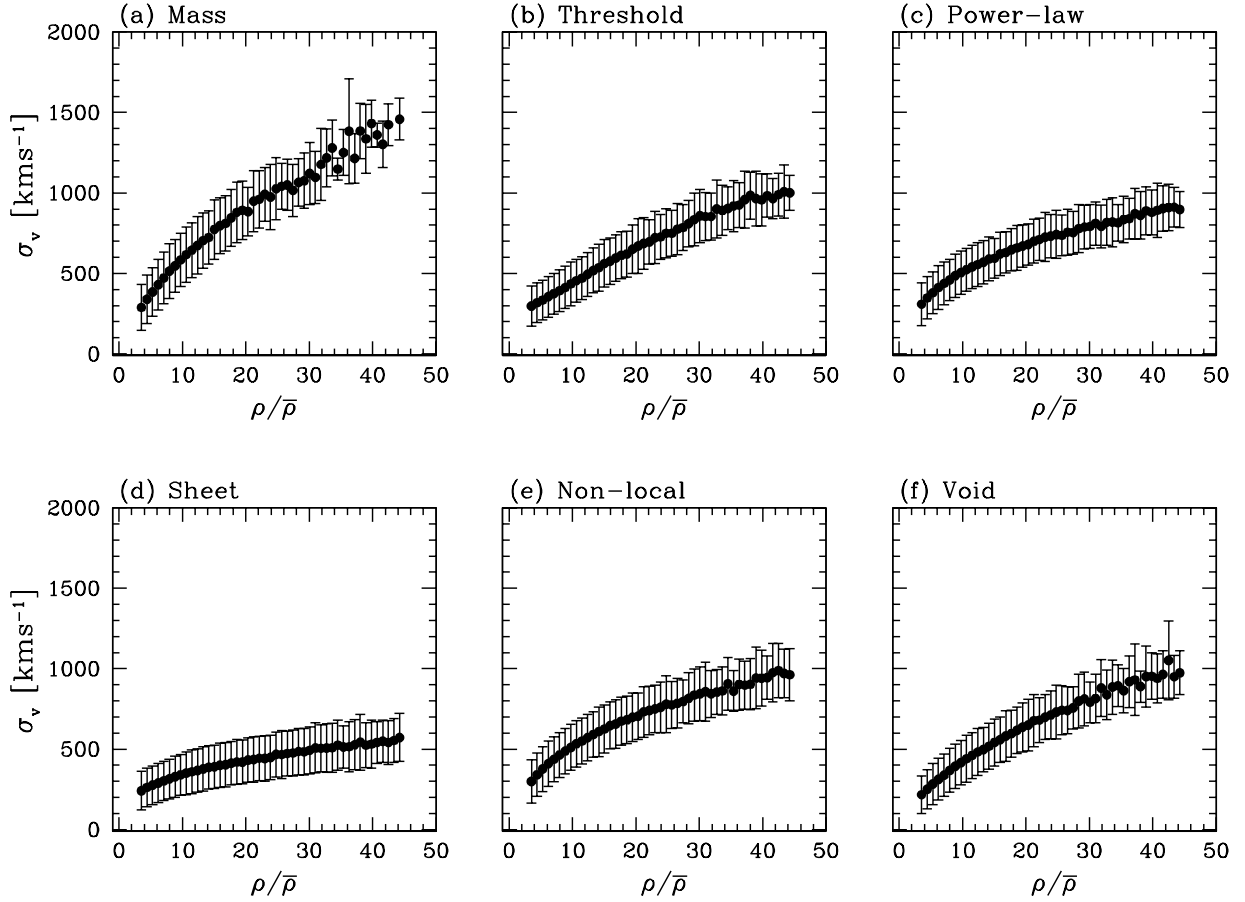


Fig. 15.— Velocity dispersion σ_v as a function of the local mass (a) or galaxy (b-f) overdensity $\rho/\bar{\rho}$. Both quantities are computed in spheres of radius $3h^{-1}\text{Mpc}$ using four independent simulations. Error bars show the intrinsic dispersion in σ_v at fixed $\rho/\bar{\rho}$, not the (small) statistical uncertainty in our estimate of the mean $\sigma_v(\rho/\bar{\rho})$.

contrast in the non-local model does not significantly increase the scatter in δ_g vs. δ_m over that in the power-law model. In the sheet bias model, on the other hand, galaxy selection is based on the geometry of the local mass distribution rather than the mass density. These quantities are correlated, but the scatter between σ_g and σ_m is much larger than in the density-based models, though it still becomes fairly small for $R_s \geq 10h^{-1}$ Mpc. In the void bias model, the probability that a mass particle is included as a galaxy is entirely independent of the local mass density, since the voids are thrown at random into the mass distribution. The void bias model therefore has large scatter between δ_g and δ_m , persisting to very large scales. At small R_s , the 10th percentile at all δ_m corresponds to regions that are empty of galaxies, while the 90th percentile corresponds to regions in which the smoothing volume does not overlap any of the voids.

In practice, the mass density contrast δ_m used as the independent variable in Figure 16 is not directly observable. However, δ_m can be inferred from the divergence of the peculiar velocity field using the linear perturbation theory relation $\delta_m = -\Omega^{-0.6}\nabla \cdot \mathbf{v}/H_0$ or weakly non-linear relations (Nusser et al. 1991; Gramann 1993; Chodorowski & Lokas 1997; Susperregi & Buchert 1997). The quantity $\nabla \cdot \mathbf{v}$ can be inferred from observations of the radial peculiar velocity field by the POTENT method, under the assumption that the peculiar velocity field remains irrotational during gravitational evolution (Bertschinger & Dekel 1989; Dekel et al. 1993; Sigad et al. 1998). In the case of linear bias, the slope of the relation between δ_g and $\nabla \cdot \mathbf{v}$ provides an estimate of the quantity $\beta = \Omega^{0.6}/b$.

Figure 17 shows the relation between δ_g and $-\nabla \cdot \mathbf{v}$ for the unbiased mass distribution (top row) and the various biased galaxy distributions, in the same format as Figure 16. The three columns from left to right show the relation when the fields are smoothed with Gaussian filters of radius $R_s = 6, 10, \text{ and } 15h^{-1}$ Mpc, respectively. We use the method of Babul et al. (1994) to create a volume-weighted, smoothed velocity field from the discrete galaxy peculiar velocities. Specifically, we first form the momentum field by CIC-binning the momentum of every galaxy onto a 200^3 grid. We smooth this momentum field with a Gaussian filter of radius $R_1 = R_s/2$ and divide it by a similarly smoothed density field to form a mass-weighted smoothed velocity field. We then smooth this velocity field with another Gaussian filter of radius $R_2 = (R_s^2 - R_1^2)^{1/2}$, so that the effective smoothing radius is R_s . Because the second smoothing dominates over the first, the final velocity field is volume-weighted rather than mass-weighted. We do not show the δ_v vs. $-\nabla \cdot \mathbf{v}$ relation at $R_s = 3h^{-1}$ Mpc because the discrete galaxy distribution yields an excessively noisy velocity field in low density regions for this smoothing length.

In the first row of Figure 17, systematic departures of the solid curves from the linear theory relation $\delta_m = -\nabla \cdot \mathbf{v}/H_0$ are caused by non-linear gravitational evolution. This deviation decreases drastically with increased smoothing, showing that linear theory is an increasingly better approximation of the gravitational evolution on larger scales. The panels in the remaining rows of Figure 17 show the distribution of the galaxy density fluctuations δ_g plotted against $-2\nabla \cdot \mathbf{v}/H_0$. For $R_s = 15h^{-1}$ Mpc these plots look similar to the corresponding panels of Figure 16. For smaller smoothing lengths the relation between δ_g and $-\nabla \cdot \mathbf{v}$ is more non-linear than the relation

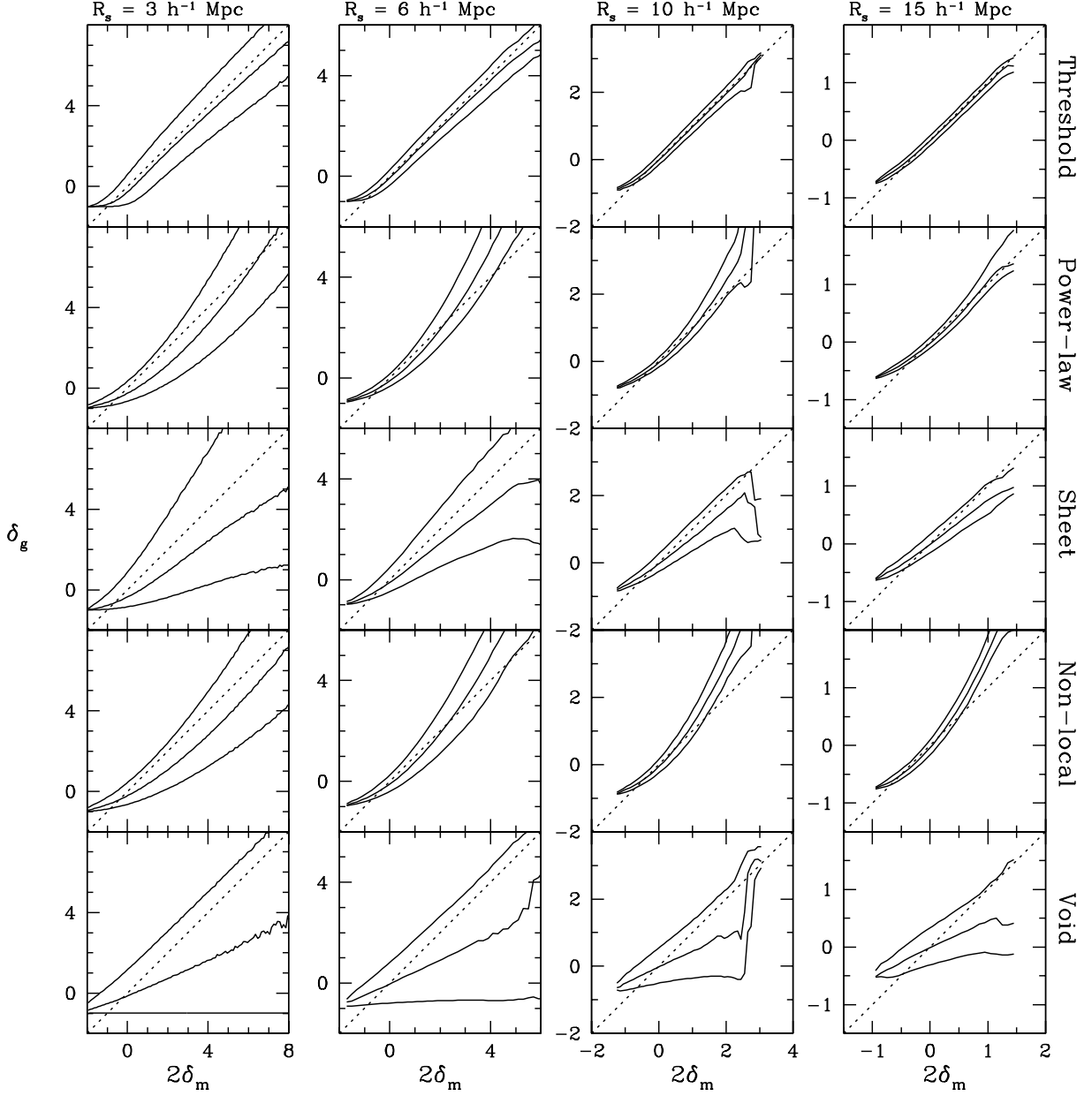


Fig. 16.— The galaxy overdensity δ_g as a function of the mass overdensity δ_m for the different biasing schemes (labeled at right). In all panels the central line shows the median relation and the upper and lower lines represent the 90th and the 10th percentile of the distribution. From left to right, the different columns show the relation when the fields are smoothed with Gaussian filters of radii $R_s = 3, 6, 10$ and $15 h^{-1} \text{ Mpc}$, respectively.

between δ_g and δ_m because of the additional non-linearity of the $\delta_g - \delta_m$ relation. Comparisons between galaxy density fields and mass density fields estimated from POTENT usually account for the non-linear relation between δ_m and $-\nabla \cdot \mathbf{v}$, but the non-linearity and scatter of the bias relation itself are potential sources of additional systematic error in POTENT estimates of β , as noted by DL98. The importance of these effects depends in detail on the form of bias — e.g., density-threshold bias produces a nearly linear relation with small scatter, power-law bias produces a non-linear relation with small scatter, and sheet bias produces a nearly linear relation with large scatter.

4. Discussion

We have examined the influence of the morphology-density relation and biased galaxy formation on many of the statistical measures that are commonly used to characterize galaxy clustering and galaxy peculiar velocity fields. We have focused most of our attention on local biasing models, in which the efficiency of galaxy formation is governed by the density (density-threshold or power-law bias), geometry (sheet or filament bias), or “pressure” ($\rho\sigma_v^2$) within a sphere of radius $4h^{-1}$ Mpc. We have contrasted the behavior of these local models with that of models in which the galaxy density is coherently modulated over large scales (non-local bias, as proposed by BCFW93) or suppressed in randomly distributed voids (void bias, as proposed by BW91). In this Section, we summarize our results, then discuss them in light of other recent work and anticipated observational developments.

If the morphological segregation of galaxies is governed by the local morphology-density relation proposed by Postman & Geller (1984), then on small scales the correlation function of early-type galaxies should be both steeper and stronger than that of late-type galaxies, in accord with present observations. On scales larger than the galaxy correlation length, early-type galaxies should remain more strongly clustered than late-type galaxies, but the correlation functions (and power spectra) should have the same shape. This prediction of the local morphology-density model is consistent with current data and can be tested at high precision by the 2dF and SDSS redshift surveys.

In all of the examples that we have investigated, local bias produces a scale-independent amplification of the two-point correlation function and power spectrum on scales in the linear regime. On these scales, therefore, local biasing cannot resolve a discrepancy between the shape of the mass power spectrum predicted by a cosmological model and the shape of the observed galaxy power spectrum. Non-local biasing can resolve such a discrepancy, as originally shown by BW91 and BCFW93 in the context of “standard” CDM and the APM galaxy survey, but achieving this alteration of the power spectrum shape requires a bias mechanism that directly modulates galaxy formation in a coherent way over large scales. In the non-linear regime, by contrast, the bias functions $b_\xi(r)$, $b_\sigma(r)$, and $b_P(k)$ are scale-dependent even in local models, and their shapes depend on the details of the biasing scheme.

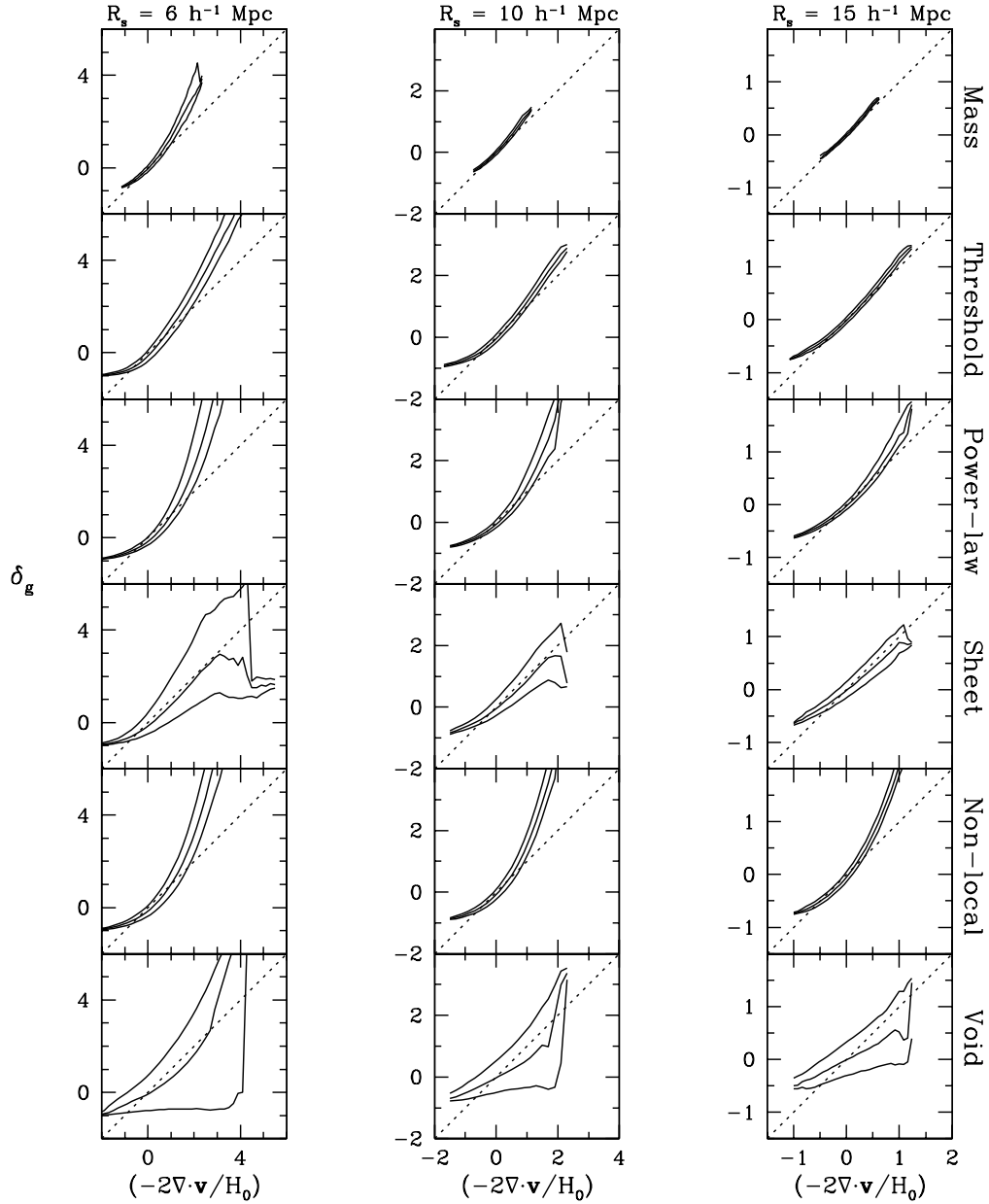


Fig. 17.— The galaxy overdensity δ_g as a function of the negative divergence of the velocity field (divided by the Hubble constant), for the mass distribution and the various biased galaxy distributions (labeled at right). In all panels the central line shows the median relation and the upper and lower lines represent the 90th and the 10th percentile of the distribution. From left to right, the different columns show the relation when the density and velocity fields are smoothed with Gaussian filters of radii $R_s = 6, 10$ and $15 h^{-1} \text{ Mpc}$, respectively. The first row of panels shows the relation between δ_m and $-\nabla \cdot \mathbf{v}/H_0$, while subsequent rows show the relation between δ_g and $-\nabla \cdot \mathbf{v}/H_0$.

Local bias models roughly preserve the hierarchical relations between moments of the galaxy count distribution, in that the ratios $S_3 \equiv \langle \delta_g^3 \rangle_c / \langle \delta_g^2 \rangle^2$ and $S_4 \equiv \langle \delta_g^4 \rangle_c / \langle \delta_g^2 \rangle^3$ are only weakly dependent on smoothing scale (and hence on $\sigma \equiv \langle \delta_g^2 \rangle^{1/2}$). However, local bias can change both the amplitude and shape of the functions $S_3(\sigma)$ and $S_4(\sigma)$. Our power-law bias model gives $S_3(\sigma)$ and $S_4(\sigma)$ close to those of the underlying mass distribution, and our non-local bias model in turn gives $S_3(\sigma)$ and $S_4(\sigma)$ close to those of the local power-law model. These results show that agreement between measured hierarchical amplitudes and perturbation theory predictions for the mass distribution does not necessarily imply that galaxy formation is unbiased or even that it is locally biased, although such agreement can rule out specific local and non-local models (Frieman & Gaztañaga 1994).

If we characterize the effect of bias on the variance and skewness of galaxy counts by linear and quadratic bias parameters b_1 and b_2 , then b_1 is independent of scale on large scales in all of our local models. Our results are marginally but not strongly inconsistent with the conjecture that b_2 becomes scale-independent on large scales in local bias models. The scale-dependence of $b_1(r)$ and $b_2(r)$ is much stronger in our non-local model than in any of our local models. On large scales, void bias produces a scale-independent $b_1(r)$ but a scale-dependent $b_2(r)$.

Estimates of moments of the velocity distribution from galaxy redshift surveys, which are weighted by galaxy pairs, are strongly affected by biasing because of correlations between the velocity distribution and the parameters that determine the galaxy formation efficiency. In particular, the pairwise velocity dispersion $\sigma_v(r)$ is sensitive to the details of the bias model at all separations. The two bias models with the steepest small scale correlation function, power-law bias and sheet bias, have values of σ_v that differ by a factor of two at $r \sim 2h^{-1}$ Mpc, because the first enhances galaxy formation in dense, isotropic clusters while the second does not. The dependence of the mean pairwise velocity $V_{12}(r)$ on bias is similarly complex on small scales, but the behavior simplifies for local bias models at large r , where the galaxy V_{12} is amplified over the mass V_{12} by a factor b_v that is close to the correlation function bias b_ξ . These biases of pairwise moments arise even though the galaxies in our models are just a subset of the dark matter particles and therefore have the same local velocity distribution. Void bias presents an odd case in which the galaxy distribution is biased but $\sigma_v(r)$ and $V_{12}(r)$ are not. The relation between local velocity dispersion and local overdensity (Kepner et al. 1997; Strauss et al. 1998) is also sensitive to bias, complicating the use of this statistic as a diagnostic for Ω .

The median trend and scatter of the relation between δ_g and δ_m or δ_g and $-\nabla \cdot \mathbf{v}$ depends on the biasing scheme and on the smoothing scale used to define the density and velocity fields. The density-threshold bias prescription produces a relation that is remarkably close to linear bias, $\delta_g = b\delta_m$. Power-law bias produces a curved $\delta_g - \delta_m$ relation, and, as noted by DL98, the non-linearity of this relation is a possible source of systematic error in efforts to measure $\beta \equiv \Omega^{0.6}/b$ via the POTENT method (Dekel et al. 1993; Sigad et al. 1998) or via redshift space distortions (Hamilton 1998 and references therein). The relation between δ_g and δ_m is fairly tight for the bias schemes that are based on local density, but it exhibits much more scatter for the

sheet bias scheme, as one might expect. The void bias model predicts very large scatter between δ_g and δ_m or $-\nabla \cdot \mathbf{v}$, even for smoothing lengths as large as $15h^{-1}$ Mpc. The observed correlation between δ_g and $-\nabla \cdot \mathbf{v}$ (Sigad et al. 1998) is probably sufficient to rule out such a model, as first argued by Babul et al. (1994). However, our less extreme non-local bias model predicts a relation that is nearly as tight as that of the local power-law bias model, so the existence of a tight relation between δ_g and $-\nabla \cdot \mathbf{v}$ is not sufficient to rule out non-locally biased galaxy formation.

Our results for the large scale behavior of $\xi(r)$ and $P(k)$ strengthen the conclusions of earlier analytic arguments (Coles 1993; Fry & Gaztañaga 1993; Gaztanaga & Baugh 1998; Scherrer & Weinberg 1998) and numerical investigations (Weinberg 1995; MPH98; Cole et al. 1998). Although we can only examine a finite number of specific biasing prescriptions, these examples show that scale-independent amplification of $\xi(r)$ and $P(k)$ occurs even in models like sheet, filament, and pressure bias, where the galaxy formation efficiency is not governed strictly by the local mass density. We also find that the asymptotic regime of nearly constant b_ξ , b_σ , and b_P is effectively reached on mildly non-linear scales, soon after $\xi(r)$ drops below one.

Our conclusions may seem mildly at odds with those of Blanton et al. (1998, hereafter BCOS98), who find scale-dependent bias of the “galaxy” population in a hydrodynamic simulation of the Λ +CDM model (by Cen & Ostriker 1998). The difference is largely a matter of emphasis: BCOS98 find substantial scale-dependence of $b_\sigma(r)$ in the non-linear regime, but they find only a 12% drop in $b_\sigma(r)$ from $r = 8h^{-1}$ Mpc to $r = 30h^{-1}$ Mpc, which is the same drop we find for our sheet bias model. Our power-law and sheet bias models also show significant scale-dependence of $b_\sigma(r)$ in the non-linear regime ($r < 8h^{-1}$ Mpc), though not as strong as that found by BCOS98. BCOS98 demonstrate that the scale-dependence of bias in their simulation arises mainly from the correlation between galaxy formation efficiency and the local gas temperature T or dark matter velocity dispersion σ_v^2 . They further argue that this correlation leads to scale-dependence because of the connection between T (or σ_v^2) and the gravitational potential, which has a much redder power spectrum than the density field itself. In the terminology of this paper, the BCOS98 argument could be rephrased as a claim that temperature is a local variable whose influence is more “effectively non-local” than that of other local variables. The fact that we obtain virtually identical results for density-threshold and pressure bias implies that enhanced scale-dependence is not an *automatic* consequence of incorporating temperature or σ_v^2 into the biasing prescription. In order to address this issue more directly, we also examined a model in which we biased the galaxy distribution using a threshold in σ_v^2 alone, a pure “temperature” bias. We again obtained results nearly identical to those of the density-threshold model, with no enhanced scale-dependence of the bias. The difference of our result from that of BCOS98’s similar numerical experiment presumably reflects our use of a $4h^{-1}$ Mpc rather than a $1h^{-1}$ Mpc sphere to define σ_v^2 . Averaged over this larger scale, velocity dispersion does not behave any more “non-locally” than density. This result does not mean that galaxy bias in a realistic model might not be as scale-dependent as BCOS98 find, only that the influence of temperature or velocity dispersion on the scale-dependence of bias depends in detail on the scale over which it is defined and the way that it is incorporated into the

bias prescription.

Our numerical study complements the general analytic examination of stochastic, non-linear biasing by DL98. The use of N-body simulations allows us to investigate the effects of a wide range of biasing prescriptions on measures of galaxy clustering in the linear, mildly non-linear, and strongly non-linear regimes. For the most part, we have addressed different issues from DL98, but we concur on the general point that bias is a multi-faceted phenomenon, and that only in specific cases and limits can it be described by a single parameter. On small scales, the relation between δ_g and δ_m is generically non-linear and scale-dependent, and it may have substantial scatter. At any given scale one can define many different “bias factors” — b_ξ , b_σ , b_P , b_1 , b_2 , b_v , etc. — and the relation among them depends on the details of the biasing scheme, or, ultimately, on the physics of galaxy formation.

Despite this complexity, our results show that the very general assumption of local biasing leads to some important simplifications on large scales. Most significantly, the scale-independence of b_ξ and b_P in the linear regime means that large galaxy redshift surveys like 2dF and the SDSS should reveal the true shape of the dark matter power spectrum on large scales, if galaxy formation is governed by local physics. Indeed, this result makes the local biasing hypothesis testable, since any non-local physics that significantly modulated galaxy formation would almost certainly have a different impact on galaxies of widely differing luminosity, stellar population age, morphology, and surface mass density. Existing data clearly show that different types of galaxies have different clustering amplitudes, but if each galaxy’s properties are determined by the history of its local environment then the 2dF and SDSS redshift surveys should show that all galaxies have the same $P(k)$ shape on large scales.

The uncertainties of bias have been a source of frustration in efforts to test cosmological models against observations of galaxy clustering. In recent years, observational and theoretical breakthroughs have opened a number of alternative routes to measuring cosmological parameters and the mass power spectrum, including microwave background anisotropies, the Ly α forest, the supernova Hubble diagram, weak gravitational lensing, and the mass function and evolution of the galaxy cluster population. These approaches are insensitive or weakly sensitive to biased galaxy formation, though each one has its own set of assumptions and limitations. Recent years have also seen great improvements in the predictive power of theories of galaxy formation, thanks to advances in numerical simulations and semi-analytic modeling techniques that combine gravitational clustering with the more complicated physical processes of gas cooling, star formation, supernova feedback, metal enrichment, and morphological transformation via mergers and interactions. While the sensitivity of galaxy clustering statistics to the details of galaxy biasing is an obstacle to testing cosmological models, it becomes an asset when the goal is testing the theory of galaxy formation itself, especially if the underlying cosmological model is tightly constrained by independent observations. We have already argued that $P(k)$ and $\xi(r)$ can test the broad hypothesis of local galaxy formation, and at a greater level of detail we might, for example, come to view the pairwise velocity dispersion not as a tool for measuring Ω but as a diagnostic for

the importance of mergers in dense environments. The giant redshift surveys currently underway will provide superb data sets for such studies, allowing precise clustering measurements for finely divided subsets of the galaxy population over a wide range of scales. Other kinds of data may play an equal or more important role in determining the material contents of the universe and the origin of cosmic inhomogeneity, but measurements of large scale structure at high and low redshift will guide our understanding of the physics that transformed primordial dark matter fluctuations into the universe of galaxies.

This work was supported by NSF Grant AST-9616822 and NASA Astrophysical Theory Grant NAG5-3111. We thank Roman Scoccimarro for helpful discussions on galaxy moments and their relation to non-linear bias factors.

REFERENCES

- Abell, G. O. 1958, *ApJS*, 50, 241
- Babul, A., & Postman, M. 1990, *ApJ*, 359, 280
- Babul, A., & White, S. D. M. 1991, *MNRAS*, 253, 31P (BW91)
- Babul, A., Weinberg, D. H., Dekel, A., & Ostriker, J. P. 1994, *ApJ*, 427, 1
- Bardeen, J., Bond, J. R., Kaiser, N., & Szalay, A. 1986, *ApJ*, 304, 15
- Bean, A. J., Ellis, R. S., Shanks, T., Efstathiou, G., & Peterson, B. A. 1983, *MNRAS*, 205, 605
- Benoist, C., Maurogordato, S., da Costa, L. N., Cappi, A., & Schaeffer, R. 1996, *ApJ*, 472, 459
- Bernardeau, F. 1994, *ApJ*, 433, 1
- Bertschinger, E., & Dekel, A. 1989, *ApJ*, 336, L5
- Blanton, M., Cen, R., Ostriker, J.P., & Strauss, M. A. 1998, *ApJ*, submitted, astro-ph/9807029 (BCOS98)
- Bouchet, F. R., Strauss, M. A., Davis, M., Fisher, K. B., Yahil, A., & Huchra, J. P. 1993, *ApJ*, 417, 36
- Bower, R. G., Coles, P., Frenk C. S., & White, S. D. M. 1993, *ApJ*, 405, 403 (BCFW93)
- Braun, E., Dekel, A., & Shapiro, P. R. 1988, *ApJ*, 328, 34
- Cen, R., & Ostriker, J. P. 1992, *ApJ*, 399, L113
- Cen, R., & Ostriker, J. P. 1993, *ApJ*, 417, 415
- Cen, R., & Ostriker, J. P. 1998, *ApJ*, submitted, astro-ph/9809370

- Chodorowski, M., & Lokas, E. L. 1997, MNRAS, 287, 591
- Cole, S., Hatton, S., Weinberg, D. H., & Frenk, C. S. 1998, MNRAS, 300, 945 (CHWF98)
- Cole, S., Weinberg, D. H., Frenk, C. S., & Ratra, B. 1997, MNRAS, 289, 37
- Coles, P. 1993, MNRAS, 262, 1065
- Colín, P., Klypin, A. A., Kravtsov, A. V., & Khokhlov, A. M. 1998, ApJ, submitted, astro-ph/9809202
- Colless, M. 1998, Phil. Trans. R. Soc. Lond. A, in press, astro-ph/9804079
- Couchman, H. M. P. 1991, ApJ, 368, L23
- Davis, M., & Geller, M. J. 1976, ApJ, 208, 13
- Davis, M., & Peebles, P. J. E. 1977, ApJS, 34, 425
- Davis, M., & Peebles, P.J.E. 1983, ApJ, 267, 465
- Davis, M., Efstathiou, G., Frenk, C. S., & White, S. D. M. 1985, ApJ, 292, 371
- Dekel, A, Bertschinger, E., Yahil, A., Strauss, M. A., Davis, M., & Huchra, J.P. 1993, ApJ, 412, 1
- Dekel, A., & Rees, M.J. 1987, Nature, 326, 455
- Dekel, A. & Lahav, O. 1998, ApJ, submitted, astro-ph/9806193 (DL98)
- de Lapparent, V., Huchra, J.P., & Geller, M.J. 1986, ApJ, L1
- Dressler, A. 1980, ApJ236, 351
- Einasto, J., Saar, E., Einasto, M., Freudling, W., & Gramann, M. 1994, ApJ, 429, 465
- Eisenstein, D. J., & Hu, W. 1998, ApJ, 496, 605
- Eke, V. R., Cole, S., Frenk, C. S. 1996, MNRAS, 282, 263
- Fisher, K. B. 1995, ApJ, 448, 494
- Fisher, K. B., Davis, M., Strauss, M. A., Yahil, A., & Huchra, J. P. 1994, MNRAS, 267, 927
- Frieman, J. A., & Gaztañaga, E. 1994, ApJ, 425, 392
- Fry, J. N. 1984, ApJ, 279, 499
- Fry, J. N., & Gaztañaga, E. 1993, ApJ, 413, 447
- Fry, J. N. 1996, ApJ, 461, L65

- Gaztañaga, E. 1992, *ApJ*, 398, L17
- Gaztañaga, E., & Baugh, C. M. 1998, *MNRAS*, 294, 229
- Gaztañaga, E. 1994, *MNRAS*, 268, 913
- Giovanelli, R., Haynes, M. P., & Chincarini, G. L. 1986, *ApJ*, 300, 77
- Governato, F., Baugh, C.M., Frenk, C. S., Cole, S., Lacey, C. G., Quinn, T. R. & Stadel, J. 1998, *Nature*, 392, 359
- Gramann, M. 1993, *ApJ*, 405, L47
- Gunn, J. E. & Weinberg, D. H. 1995, in *Wide Field Spectroscopy and the Distant Universe*, eds. S. Maddox & A. Aragón-Salamanca, (Singapore: World Scientific), 3 (astro-ph/9412080)
- Guzzo, L., Strauss, M. A., Fisher, K. B., Giovanelli, R. & Haynes, M. P. 1997, *ApJ*, 489, 37
- Hamilton, A. J. S. 1988, *ApJ*, 331, L59
- Hamilton, A. J. S. 1998, in *Ringberg Workshop on Large-Scale Structure*, ed. D. Hamilton, (Kluwer: Dordrecht), astro-ph/9708102
- Hubble, E.P. 1936, *The Realm of the Nebulae* (Oxford University Press: Oxford), 79
- Juszkiewicz, R., Bouchet, F. R., & Colombi, S. 1993, *ApJ*, 412, L9
- Juszkiewicz, R., Weinberg, D. H., Amsterdamski, P., Chodorowski, M., & Bouchet, F. 1995, *ApJ*, 442, 39
- Kaiser, N. 1984, *MNRAS*, 294, L9
- Katz, N., Hernquist, L., & Weinberg, D. H. 1992, *ApJ*, 399, L109
- Katz, N., Weinberg D. H., & Hernquist, L. 1996, *ApJS*, 105, 19
- Katz, N., Hernquist, L., & Weinberg, D. H. 1998, *ApJ*, submitted, astro-ph/9806257
- Kauffmann, G., Colberg, J. M., Diaferio, A., & White, S. D. M. 1998, *MNRAS*, submitted, astro-ph/9805283
- Kauffmann, G., Nusser, A., & Steinmetz, M. 1997, *MNRAS*, 286, 795
- Kepner, J. V., Summers, F. J., & Strauss, M.A. 1997, *New Astron*, 2, 165
- Kim, R. S., & Strauss, M. A. 1998, *ApJ*, 493, 39
- Lahav, O., Nemiroff, R.J., & Piran, Y. 1990, *ApJ*, 350, 119
- Lahav. O., & Saslaw, W.C. 1992, *ApJ*, 396, 430

- Little, B., & Weinberg, D. H. 1994, MNRAS, 267, 605
- Loveday, J., Maddox, S. J., Efstathiou, G., & Peterson, B. A. 1995, ApJ, 468, 442
- Maddox, S. J., Efstathiou, G., Sutherland, W. J., & Loveday, J. 1990, MNRAS, 242, 43P
- Mann, R. G., Peacock, J.A, & Heavens, A.F. 1998, MNRAS, 293, 209 (MPH98)
- Meiksin, A., Szapudi, I., & Szalay, A. 1992, ApJ, 394, 87
- Melott, A. L., & Fry, J. N. 1986, ApJ, 305, 1
- Mo, H. J., Jing, Y. P., & Borner, G. 1993, MNRAS, 264, 825
- Nusser, A., Dekel, A., Bertschinger, E., & Blumenthal, G. 1991, ApJ, 379, 6
- Ostriker, J. P., & Cowie, L. L. 1981, ApJ, 243, L127
- Park, C., 1990, PhD Thesis, Princeton University.
- Park, C. 1991, MNRAS, 251, 167
- Park, C., Vogeley, M. S., Geller, M. J., & Huchra, J. P. 1994, ApJ, 431, 569
- Peacock, J. A., & Dodds, S. J. 1994, MNRAS, 267, 1020
- Peebles, P. J. E. 1976, ApJ, L109
- Postman, M., & Geller, M.J. 1984, ApJ, 281, 95 (PG84)
- Saunders W., Rowan-Robinson, M., & Lawrence, A. 1992, MNRAS258, 134
- Scherrer, R. J., & Weinberg, D. H. 1998, ApJ, 504, 607
- Sigad, Y., Eldar, A., Dekel, A., Strauss, M. A., & Yahil, A. 1998, ApJ, 495, 516S
- Somerville, R., Primack, J., & Nolthenius, R. 1997, ApJ, 479, 606
- Strauss, M.A., Ostriker, J.P., & Cen, R. 1998, ApJ, 494, 20
- Susperregi, M., & Buchert, T. 1997, A&A, 323, 295
- Sugiyama, N. 1995, ApJS, 100, 281
- Tegmark, M., & Peebles, P,J,E. 1998, ApJ, submitted
- Vishniac, E., Ostriker, J. P., & Bertschinger, E. 1985, ApJ, 291, 399
- Weinberg, D. H. 1995, in Wide-Field Spectroscopy and the Distant Universe, eds. S. J. Maddox and A. Aragón-Salamanca (Singapore: World Scientific), 129

White, S. D. M., Efstathiou, G. P., & Frenk, C. S. 1993, MNRAS, 262, 1023

White, S. D. M., & Ostriker, J. P. 1990, ApJ, 349, 22

Whitmore, B. C., Gilmore, D. M., & Jones, C. 1993, ApJ, 407, 489

Willmer, C. N. A., da Costa, L. N., & Pellegrini, P. S. 1998, AJ, 115, 869

Zurek, W. H., Quinn, P.J., Salmon, J.K., & Warren, M.S. 1994, ApJ, 431, 559

Zwicky, F. 1937, ApJ, 86, 217